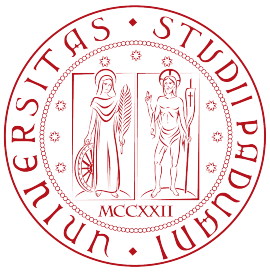

UNIVERSITÀ DEGLI STUDI DI PADOVA

Dipartimento di Fisica e Astronomia "Galileo Galilei"

Corso di Laurea Magistrale in Astronomia

Tesi di Laurea Magistrale

Satellite Navigation System with Pulsars

Relatore:
Prof. Giampiero Naletto

Laureanda:
Francesca Brotto

Correlatori:
Prof. Luca Zampieri, Dott. Paolo Zoccarato

Anno Accademico 2018-2019

Contents

Abstract

The aim of this Thesis is assessing the feasibility and the accuracy achievable through navigation systems for satellites aided with optical pulsars. Pulsar navigation systems can provide an autonomous method for the determination of position, velocity and attitude of spacecraft for any interplanetary missions. To date, satellite navigation is not done in an autonomous way. For this reason we are interested in looking into an autonomous navigation system. The idea is to take advantage of the extremely high precision of pulsar signals and to use them as natural navigation beacons. Using pulsars to navigate deep space has already been proposed and already tested in orbit. However, no previous studies focussed on the idea of using the optical emission of these types of sources. For this purpose, the available optical sources, the usable navigation techniques and their accuracies have been studied. We followed two directions. On one hand, accuracy analyses have been performed to determine the main uncertainties that affect most the accuracy of the position determination. On the other hand, an analysis on real ground data of the optical pulse of the Crab nebula pulsar has been performed. The results of this preliminary study are encouraging in the sense that it seems possible to navigate in space with the help of optical pulsations of the pulsars with a better accuracy than that achieved using X-ray pulsars. However, further studies are needed to define the necessary tools and useful software to navigate in space with the help of optical pulsars.

1. Introduction

The idea that once again humankind needs to look up to the sky to navigate is really fascinating, and the fact that this time men need to use stars for space flight is even more attractive.

An autonomous navigation system for the Solar System could be really interesting for any kind of existing and future spacecraft missions. Currently navigation of satellites is not possible in an autonomous way. Satellite navigation is largely done by means of a large number of ground based radio telescopes that communicate with the satellites in interplanetary space via telemetry. Therefore, satellites navigate in space thanks to networks of radio telescopes (for example DSN the NASA deep space network or ESTRACK, European Space Tracking, the ESA deep space network) that send signals from Earth; but if the number of spacecraft that navigate in space increases in future, a bigger network will be needed, that means difficult and expensive work. A solution to this problem would be to allow spacecraft to calculate its own position, hence autonomous navigation. Pulsar stars could be a good aid to achieve autonomous navigation. These sources can be called lighthouses in the sky because of their extremely stable and periodic signals. The idea of using these sources as navigation beacons for an autonomous navigation system derives from the particularities of their signals. In fact, they beam periodic signals that have timing stabilities comparable to atomic clocks and provide characteristic temporal signals that can be used as natural navigation beacons. Ideally, the position of the spacecraft can be determined autonomously and with high accuracy everywhere in the Solar System and beyond.

In order to investigate in the best possible way this interdisciplinary problem an internship at the European Space Technology and Research Centre (ESTEC) has been performed. The internship lasted two months during which the issue was investigated and the reasons of the interest in this topic were understood. The work undertaken over these two months has been continued for additional months at Padova University.
The aim of this thesis is the feasibility of an autonomous navigation system for satellites with the help of pulsar stars. To investigate on this topic several steps needed to be pursued. First of all the study of pulsar stars and of particular features that make these sources interesting for satellite navigation has been done. Their particular stable timing makes these sources possible natural navigation beacons for an autonomous navigation system. However, these sources show timing noise that can limit the accuracy of the process to determine the position. Furthermore, these

sources emit very weak signals which make their detection difficult considering the small feasible dimensions of the telescope for a spacecraft. Chapter 2 describes these sources and in particular it focuses on the physical properties useful to understand why there is the idea of using pulsar stars as natural beacons. After the description of the functional characteristics of these sources, the current usable navigation systems have been described. Chapter 3 focuses on this topic: the different current navigation techniques, which depend on the type of mission, are described. There are two main types of navigation techniques: in the case of LEO (Low Earth Orbit) satellites the position is determined by the usage of systems similar to those used to determine the position on the ground, while in the case of satellites that navigate in deep space there are networks of radio-telescopes for tracking the satellites from Earth. Moreover, in this chapter a detailed introduction about the historical notes of pulsar navigation system is reported. This introduction is useful to understand why we choose to study feasibility of pulsar navigation systems using the optical emission of these sources. To date all the studies carried out concerning satellite navigation with pulsars have considered radio or X-ray pulsars. Our idea is to use optical pulsars, instead of radio or X-ray ones, because of the improvements that a greater number of photons can bring to the navigation system. Chapter 4 focuses on the theory behind optical pulsar navigation. The basic concept of the pulsar navigation system is here described. Pulsars timing analysis is linked to the determination of the Time of Arrival (ToA) of the pulsar photons at the detector. It is straightforward that the measurements of the ToA are closely linked with position and velocity of the detector in space. In fact, a delay of the ToA of the photons is equivalent to the light delay between the real position and the estimate position along the line of sight of the pulsar. Moreover, the two different possible usable pulsar navigation methods are pointed out: the phase measurement and the significance analysis. After the description of the techniques and the problems with each technique, an analysis on the available optical pulsars has been carried out. Chapter 5 reports all the available optical sources and the description of each of them. In detail, the description is useful to understand which optical pulsars are the best candidates for the pulsars navigation system. The pulsar of the Crab nebula has been identified as the best optical pulsar candidate. For a pulsar navigation system the distribution of pulsars in the sky is important: in this chapter the distribution of optical pulsars has been described. One of the navigation techniques needs to observe more than one pulsar at a time: in order to determine if it is possible to do so, an example of visibility analysis has been performed. Furthermore, it is reported here a first analysis about the achievable accuracy on the position determination with the Crab pulsar considering different telescope diameters. Only after the definition of the concept of pulsar navigation, the different methods that can be used to determine the spacecraft position, the description of the available optical pulsars, and the selection of the best candidates for the purpose, it is possible to perform the accuracy analyses. Chapters 6 and 7 deal with the results of this thesis work. In order to reach the purpose of the thesis we acted in two directions. Chapter 6 deals with the results of the accuracy analyses of the phase measurement navigation method. They are done to analyse the uncertainty which influence most the accuracy of the position determination process, moreover they are also done to investigate the achievable accuracy on position and

velocity determination of the spacecraft using optical pulsar as navigation beacons. The covariance matrices of the system have been calculated using two different estimate theories. The first method is an epoch-by-epoch approach which means that the position of the spacecraft is determined using single observation of the pulsars. The weighted least squares estimate theory allows this type of analysis. The best result of this analysis is accuracy of 10 km obtained using 9 pulsars. In order to verify that it was possible to obtain better accuracy another approach has been performed. The second method is an iterated approach, which means that the position of the spacecraft is continuously determined by observing pulsars continuously. The extended Kalman filter estimate theory permits this type of analysis. The best result obtained with this estimation theory is $\sim 5 \times 10^2$ m after 20 days of iterated observation with a sampling time of 10 s. In both cases the main result is that the accuracy of the position determination process is mainly due to the uncertainty of the pulse profile which is due to the intrinsic timing noise of the pulsars. The intrinsic timing noise of the pulsars is not easy to model and to predict. In order to verify and to try to improve the results of the a-priori accuracy analyses, an analysis with real data of the Crab pulsar has been performed. In Chapter 7 the results of this analysis have been reported. The data utilized are ground data taken with the 182 cm Copernicus telescope of the Asiago observatory of the Crab pulsar. The aim of this analysis was to verify the a-priori accuracy analyses reported in Chapter 6 and to understand what are the main problems with optical pulsar navigation systems. The analysis performed deals with the phase measurement and the significance analysis methods. The obtained results confirm those of the previous analysis: the main uncertainty is due to timing noise of the pulsars. However, the obtained results show a better accuracy in the position determination with the two methods with respect to the a-priori accuracy analyses. The phase measurement method shows that it is possible to measure a shift of the spacecraft from the real position even of only 3000 m. The significance analysis gives an uncertainty of 1335 m in the position determination. However, to perform these analyses various assumptions have been made and further analyses are needed. Chapter 8 summarizes the results reported in Chapters 6 and 7 and reports the important remarks of this work. Moreover it describes what are the future analysis that can be done in order to continue research on this topic. In detail, it can be said that the purpose of the thesis, which was the feasibility of a satellite navigation system using optical pulsars, has been successfully achieved. However, further studies are needed to define the necessary tools and useful software to navigate in space with the help of optical pulsars.

2. Pulsars

Pulsars are the sources that are proposed to be adopted as natural navigation beacons in a new satellite navigation system. In this chapter pulsars are introduced and the properties, needed to understand the problem, are described in detail.

2.1 History and Discovery

The history of pulsars is quite recent, being the first pulsar discovered in 1967.
The idea of the existence of neutron stars was first proposed by Baade and Zwicky [1934], soon after the discovery of the neutron by Chadwick in 1932. They suggested that these stars would have a very high density, a small radius and be much more gravitationally bound compared to ordinary stars. They pointed out that neutron stars would be formed in supernova explosions and suggested that the extreme pressure in the centre of the explosion would be sufficient to trigger an inverse beta decay, during which electrons and protons are combined to form neutrons and neutrinos. Later the scientists Oppenheimer and Volkov calculated the expected size and mass of this kind of objects. The results were 10 km of radius and $1.5M_{\odot}$, where $M_{\odot}$ stands for Solar masses [Shapiro and Teukolsky, 1983]. The final consideration was that these sources were too small and their residual thermal radiation was too faint to be detected at astronomical distances with optical telescopes. After the hypothesis of Baade and Zwicky, it was necessary to wait until 1967 to discover the first pulsar (PSR B1919+21) [Hewish et al., 1968]. The research group, that made the discovery, wanted to study the scintillation of quasars in the radio band, window that had just been opened to the astronomical exploration. In fact, the first astronomical object emitting periodic pulses in the radio band was discovered by Jocelyn Bell. Anthony Hewish, who was her supervisor and the head of a group of Cambridge astronomers, earned the Nobel Prize for this discovery in 1974. At the beginning, because of the small size of the emitting source and the periodicity of the signal, the possibility that it could be a signal from an extraterrestrial civilization was considered; the source was then called LGM1 (Little Green Man 1). Soon after, Professor Hewish and his student Bell understood that it could not be an extraterrestrial source because similar events were measured in different parts of the sky and the orbital motion of the emitting source was not detected. However, the identification of this source with a neutron star was not immediate. In fact, the first astrophysicist who pointed out that the observed pulsars were rotating neutron stars was Gold [1968]. The actual observational evidence dates to 1969 with the discovery of the association of the Crab pulsar with the supernova remnant called Crab Nebula. Knowledge about op-

tical emission properties of neutron stars has remarkably improved only after the $80's$. Prior to the beginning of the $80's$, only two among the ~ 500 isolated neutron stars at that time detected as radio pulsars had been identified also at optical wavelengths [Mignani et al., 2000]. These two were the Crab pulsar (PRS B0531+21), the first optical pulsar to be discovered in 1969 [Cocke et al., 1969], and the Vela pulsar (PSR B0833-45), discovered in 1977 [Wallace et al., 1977].

2.2 Physical Properties

A pulsar is a highly magnetized fast rotating neutron star that emits beams of broadband electromagnetic radiation out of its magnetic poles along narrow emission cones, as can be seen in the representation in Figure 2.1. Radiation can be observed only when a beam of emission is pointing toward our line of sight [Ghosh and Lamb, 1992].

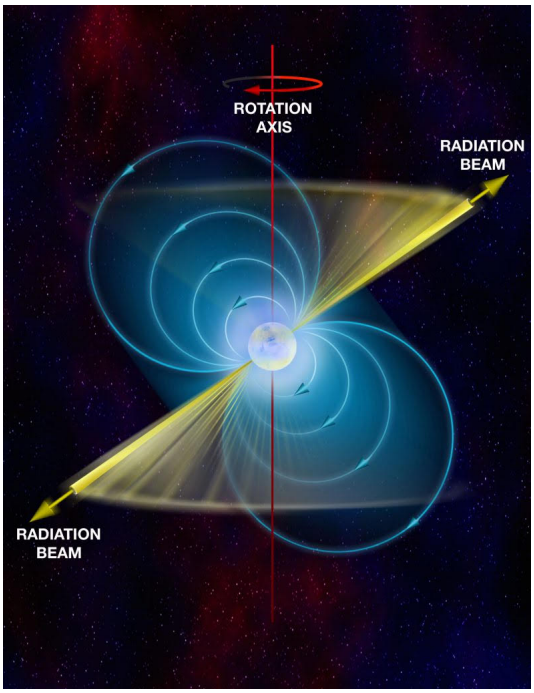

Figure 2.1: Representation of a pulsar. It can be observed that the axis of rotation and the magnetic dipole axis are not aligned. Credit: B. Saxton, NRAO\AUI\NSF.

Stars are stable as long as there is an equilibrium between the outward directed thermal pressure, caused by the nuclear fusion that occurs in the inner region, and the inward directed gravitational pressure. The stellar evolution depends mainly on the mass of the progenitor star. Neutron stars are formed from the collapse of the nucleus of a massive star at the end of its life, when its nuclear fuel is exhausted. Stars with masses in the range of about 8 to $25 - 30\ M_{\odot}$ form neutron stars from their collapse. The binding energy released from the collapse of the core produces a supernova explosion during which the bulk of the progenitor star is expelled into the interstellar medium. At the end of the gravitational collapse a very compact object

with a radius of the order of $10km$ and a mass of the order of $1.4\ M_{\odot}$ remains [Becker et al., 2013]. The star collapses so much that protons and electrons combine to form neutrons; hence the name *Neutron Star*. The collapsed star, which has drastically decreased its radius due to gravitational collapse, is born with an extremely high rotation period thanks to the conservation of angular momentum. Therefore, pulsars are rapidly rotating neutron stars. They also have a strong magnetic field and emit a collimated beam of radiation. The emission, that comes from the magnetic poles of the star, is observed if this narrow radiation cone crosses the observer's line of sight. The source behaves like a cosmic lighthouse and an observer will see a sequence of regular pulses; hence the name *pulsar* standing for Pulsating Radio Source. The properties that characterize isolated neutron stars are the spin and the magnetic field. The magnetic fields of these sources are very intense and can be of the order of 10^8 to $10^{15}G$. Pulsars periods range from *milliseconds* to *seconds* and increase very slowly. Pulsars behave as rotating magnetic dipoles that emit energy at the expense of their rotational energy hence decelerating in time. Other mechanisms contribute to the deceleration and the entire picture is not completely understood yet. The breaking torque is modelled using a power-law relation between the frequency of rotation and its derivative. The breaking index values can be determined only with long term measurements. The period signals of pulsars have *timing stabilities* comparable to atomic clocks mainly because of their isolated environments, and very large and stable moments of inertia. However, some time irregularities have been found upon long term monitoring of pulsars [Ghosh and Lamb, 1992]. There exists different types of irregularities in pulsars clocks. The period can decrease because of *glitches*, which are events that occur occasionally and are not predictable. *Glitches* are unpredictable changes in the rotational period that can be interpreted as changes in the pulsar environment or in the neutron star interior. When a glitch occurs the rotation rate suddenly changes and a period of relaxation follows before the braking index reaches a stable value [Čadež et al., 2016]. Hobbs et al. [2010] made a comparison of a large number of pulsars to demonstrate that the evolution of the rotational phase of young pulsars is dominated by long relaxation periods following significant glitches whereas older pulsars show a quasi-periodic behavior with phase modulations on typical timescales between one and ten years. Another type of timing irregularities in the pulsar timing is the *timing noise* which consists of low-frequency structures in the phase residuals, more gradual deviations from the regular spin-down compared to the glitches. The timing noise typically acts on timescale of several days or weeks, and its cumulative effects on accurate measurements of the pulse profiles on such baselines should then be taken into account.

Pulsars can be distinguished into three different classes [Ghosh and Lamb, 1992]

- *Accretion powered pulsars*: they are binary systems composed of a neutron star and a normal star. The neutron star accretes matter from the companion, gaining energy and angular momentum. These sources usually emit X-rays and their spin behavior can be very complicated with an unpredictable evolution of the rotation period. They can be very bright sources but often unsteady, with a non-coherent timing behavior caused by the the interaction of the pulsar magnetosphere with the accretion disk.

- *Magnetars*: they are isolated neutron stars. The magnetic fields of these sources are extremely high up to $\sim 10^{15}G$. The emission comes from the decay of the strong magnetic field and they are mostly X and gamma rays emitters. Their long-term timing behavior is not well determined yet.

- *Rotation powered pulsars*: they can be found in isolated or in binary systems. The emission is broadband: from the radio band up to optical, X-ray and gamma-ray band. The spin period increases, i.e. the pulsar spins down, as the rotational energy is radiated away. The electromagnetic radiation originates from the rotational energy. Two different types of rotation powered pulsars can be distinguished:

  i. ordinary isolated pulsars: most of the pulsars are of this kind and they are characterized by periods between tens of milliseconds to several seconds;

  ii. millisecond pulsars: a fraction of pulsars is of this kind and they are characterized by periods below tens of milliseconds. These pulsars have a significant timing stability and a low spin down rate. They are much older than the other pulsars. Usually they are found in non-interactive binary systems but this does not affect their stability.

Astronomers describe the life cycles and properties of the radio pulsars using the $P - \dot{P}$ diagram (see Figure 2.2), where the $\dot{P}$ is the time derivative of the rotational period P. The straight lines in the diagram represent values of constant age and

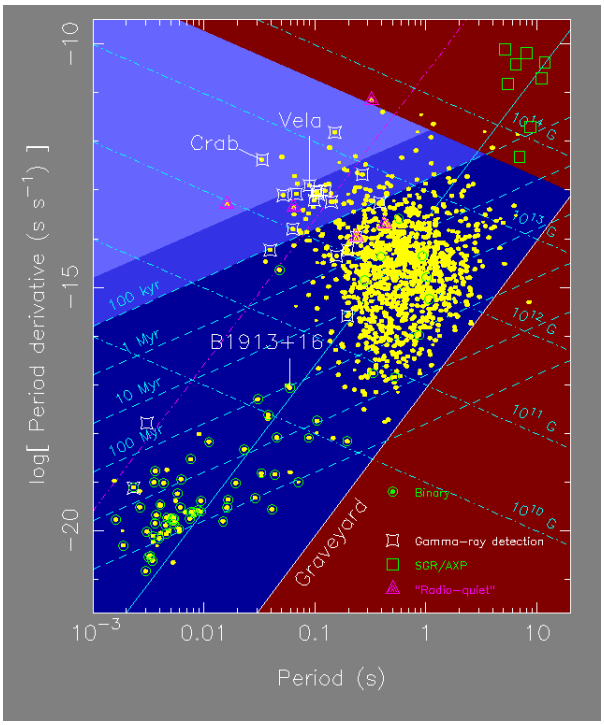

Figure 2.2: A $P - \dot{P}$ diagram. Credit: Jodrell Bank observatory (http://www.jb.man.ac.uk/).

magnetic field. Pulsars are born with short periods and slow down fast when they are young. This leads to a large $\dot{P}$ value. In the upper left part of the diagram we find

pulsars that are still associated with their supernova remnants, hence the younger ones. The older pulsars can be found in the centre of the diagram. The millisecond pulsars, that are the most stable and the oldest, can be found in the bottom left part of the diagram, with very small $\dot{P}$ values.

2.2.1 Emission Mechanism

The mechanism by which pulsars convert the rotational energy into the observed pulses is still poorly understood [Ghosh and Lamb, 1992].
The first pulsars were discovered as radio pulsating sources. In the catalogues the common abbreviation PSR stands for Pulsating Source of Radio. Soon after they were also detected in other observational bands (see Figure 2.3).

Figure 2.3: A composite image of the Crab pulsar at optical, infrared and X-ray wavelengths. Credit: NASA's Chandra: http://chandra.harvard.edu/photo/2018/crab/

Our interest is in the *optical emission* of pulsars. There are different emission mechanisms depending on the age of the pulsar. For young pulsars the optical emission is synchrotron radiation from relativistic particles which spiral around the magnetic field lines. For middle-aged pulsars there is the synchrotron radiation and the thermal radiation from the cooling neutron star surface. It is known that the basic energy source is the pulsar rotational energy, which is transferred into low-frequency radiation and the acceleration of charged particles. The uncertainty concerns the acceleration mechanism of the relativistic wind, in particular where the acceleration occurs. To constrain the theories on the spatial distribution of the emission regions it is fundamental to observe the pulsars in different wave bands [Zampieri et al., 2011]. As a matter of fact, an arrival time delay between the measurements in different bands (optical, radio or X-ray) implies that the emission regions differ in position. Actually a delay between the radio and the optical measurements has been observed in the Crab pulsar. In particular the optical pulse leads the radio one measured by

e.g. Zampieri et al. [2014] and references therein. Also the pulse profiles in the radio and optical bands differ.

2.2.2 Timing Analysis techniques

The evolution in time of the pulsar rotational period is studied using dedicated timing techniques [Ghosh and Lamb, 1992]. They are very similar in the radio, optical or higher energy bands. We will extensively use the *epoch-folding* technique to reconstruct the pulse profile. The basic concept of the epoch-folding technique is to average the profile over a number of intervals equal to the number of periods contained in a given observation. Detectors for timing are designed to measure the

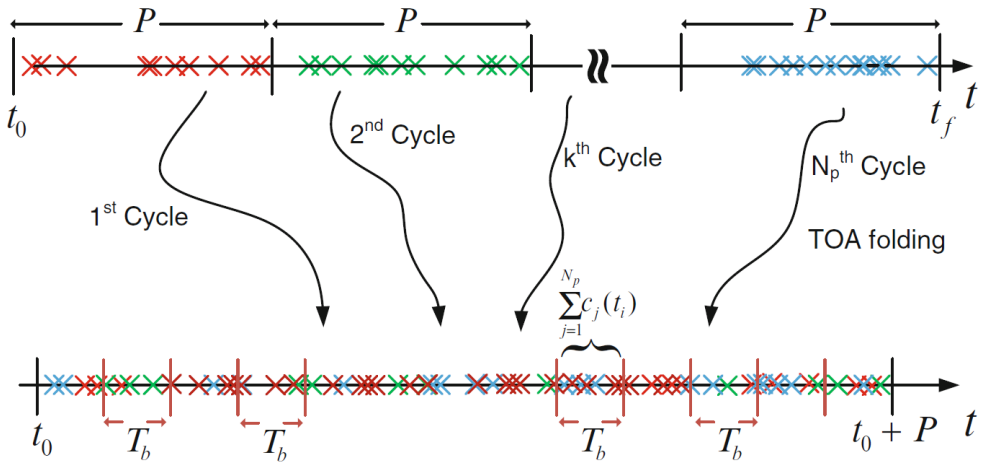

Figure 2.4: Epoch folding: the time tags photons are folded back into the first cycle $[t_0, t_0 + P]$ (with P period of the pulsar) and it is divided into N_b number of equal length bins (with size $T_b = P/N_b$). At the end the number of photons in each bin is counted and normalized [Emadzadeh and Speyer, 2010].

Time of Arrival (ToA) of photons when they hit the detecting material. A single photon counting detector permits to time tag the arrival time of each photon with a high accuracy. Epoch-folding is then applied to sources of predetermined period to determine their pulse shape. After all the time tags are collected during an observation, they are folded back into a single time interval $[t_0, t_0 + P]$ equal to one pulse period P. The period duration is divided into N_b number of equal length bins of size T_b and the number of photons in each bin is determined (see Figure 2.4). The computed photon counts are normalized and the measured pulsar profile is derived. There is the possibility to determine with high accuracy the period of a periodic time series given an initial value of the period. The method consists in folding the time series with slightly different periods in order to find through the least squares the value of the period that maximizes the quality of the fit.

3. Satellite Navigation

In this chapter current navigation systems used by satellites and related problems are investigated. In addition, the current state of art of navigation systems with the help of pulsars are investigated.

3.1 Current Navigation Systems

The current various methods used to navigate in space are listed. The methods depend on the duration and the altitude above Earth of the navigating spacecraft:

- LEO (Low Earth Orbit) is an Earth-centered orbit with an altitude of about 2000 km. Those satellites that are in such orbit can use the *GPS* (Global Positioning Satellite) system for determining the position and the velocity with 10 m and 0.01 mms^{-1} accuracy respectively [Bauer et al., 1998 IEEE]. Actually, the precision of the position determination depends on various factor: if it is done in real-time on-board or in post-processing, if it uses one or more frequencies of observation of the GNSS (Global Navigation Satellite System) signals, if it also uses the phase measurements or only those of pseudo-range [Giordano et al., 2017]. To date the achievable accuracy of the position determination in real-time on-board can ideally be of $\sim$ 10 cm. The USA's *GPS*, the European's *GNSS* (Global Navigation Satellite System), the Russia's *GLONASS* (GLObal NAvigation Satellite System) and the China's *Beidou* (which is the Chinese for Big Dipper) are all satellite navigation systems that provide continuous positioning over the globe. All these systems consist of different constellations of satellites orbiting in medium Earth orbit that provide time-stamped and coded signals [Subirana et al., 2013]. Any satellites, in a maximum altitude orbit of 20000 km, which has suitable receiver can use these systems to navigate the space. GNSS receiver consists in two parts: the antenna receives satellite signals while the processing unit analyzes it. To determine the position of the receiver satellite at least three satellites signal needs to be collected. This method is not suitable for interplanetary trajectories, in fact the satellites for the global navigation are at a maximum altitude of about 24000 km.

- For deep space missions there is one main method for navigation, the *radiometric positioning*. The spacecraft is tracked by a network of large radio telescopes from Earth. For example, the NASA's Deep Space Network (DSN) is NASA's international array of giant radio antennas that supports interplanetary spacecraft missions and for the same purpose there is the ESA's European Space

Tracking (ESTRACK). The DSN is also used for radio astronomy observations. It is important that this array permits to constantly communicate with spacecraft. To do so the DSN consists of three facilities spaced equidistant from each other around the world, before a distant spacecraft sinks below the horizon at one DSN site another site can pick up the signal. This method is not an autonomous navigation system and although accurate, precision of the determination of the position degrades according to the distance from Earth. Furthermore, the signal delay between the ground network and the spacecraft increases with distance, which therefore leads to long waiting times between one communication and another. In addition it requires a large number of systems with multiple large radio antennas to interact with, and as the number of interplanetary missions will increase so will the number of the required systems. The angular precision is of the order of 10 nrad which corresponds to a position accuracy of about 1.5 km for a distance of 1 UA from Earth [Thornton and Border, 2003].

- Using an *INS* (Inertial Navigation System), which is based on accelerometers and gyroscopes, it is possible to estimate the spacecraft's position, velocity and attitude starting from a set of initial time and position data. The instrumentation does not make use of any external information hence this is an autonomous navigation system. An INS keeps track of the position by measuring acceleration (accelerometers) and rotation (gyroscopes), from the input position and by measuring the accelerations and rotations and integrating them into speed and direction the position is tracked. The precision diminishes with time due to small inaccuracies in the measurements hence the method is not suitable for long missions [Lawrence, 1998].

3.2 Pulsar Navigation Systems

Pulsar navigation systems can provide an autonomous method for the determination of the position, the velocity and the attitude of spacecraft. This kind of navigation system sees pulsar stars as natural navigation beacons (see Figure 3.1).

3.2.1 Introduction

In this section a general introduction on the pulsar navigation system is reported. The detail of the techniques are described later in the document. This introduction is useful to understand the reasons why optical pulsars have been considered.

The idea of using pulsar stars as natural beacons to navigate in space dates back to the $70's$, soon after their discovery, when Downs [1974] proposed for the first time to use pulsating sources for interplanetary missions. The idea is to take advantage of the extreme high precision of the pulsar signals. Downs proposed to use radio sources and he showed that an accuracy of 1500 km could be obtained after 24 h of observation time. Accuracy could be improved if better radio antennas were available. Because large antennas were required, Chester and Butman [1981] gave the

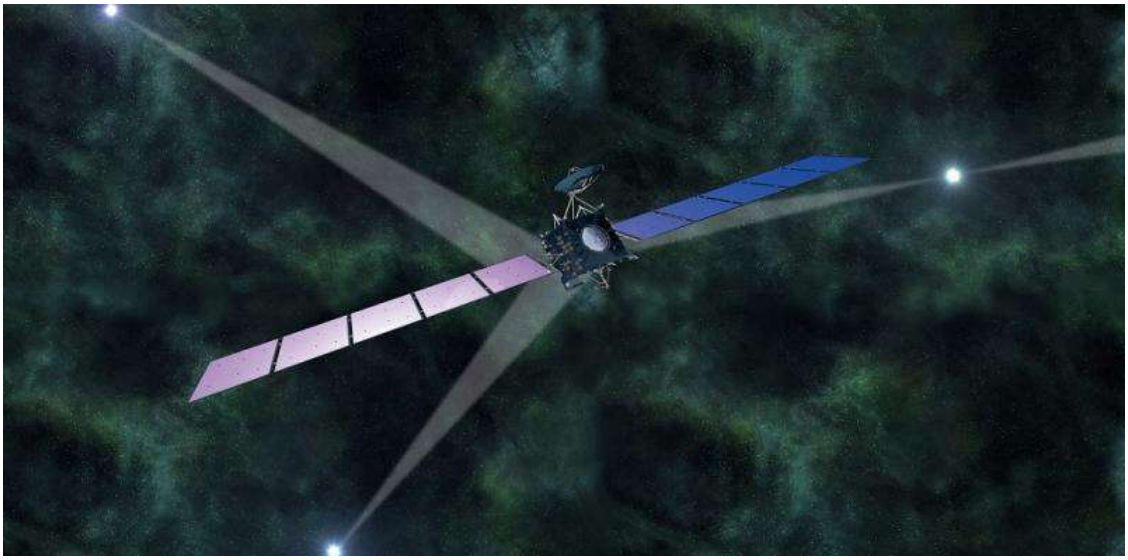

Figure 3.1: Representation of Rosetta satellite navigating if it navigated in deep space using pulsars as navigation beacons [Becker et al., 2013].

idea of using X-ray pulsars. Using X-ray pulsars instead of the radio ones makes it possible to reduce the collecting area. The determination of the position was estimated to be of about 150 km within 24 h of observation time using a detector of 0.1 m^2 collecting area. The estimation was not based on simulation or pulsar timing analyses. These early studies were not seriously considered applicable as a new autonomous navigation system. Later the improvements of knowledge of the emission properties of the pulsars and the improvements of the technology rekindled interest in the subject. Furthermore, the need for an autonomous navigation system for future interplanetary missions makes this topic intriguing for the outlets it could bring.

The basic concept for spacecraft navigation using pulsar was set out by Sala et al. [2004], Sheikh et al. [2006], Sala et al. [2008], Emadzadeh and Speyer [2010]. A large number of feasibility studies, researches, simulations and in-orbit demonstrations have been carried out considering radio and X-ray pulsars. Pulsars are usually discovered and observed using large ground-based radio telescopes, consequently the first idea was a radio navigation system. The main problem with this navigation system is the dimensions of the antenna required in order to determine the position within a reasonable observation time. For example, Becker et al. [2013] calculated phased-array radio antennas of at least 150 m^2 antenna area to make feasible spacecraft navigation with pulsars. The conclusions of that paper show that X-ray navigation system using millisecond pulsars is certainly better for the instrumentation dimensions and for the achievable accuracy. As soon as X-ray pulsar astronomy became possible by means of space telescopes, using X-ray pulsars seemed to be the solution for an autonomous system. X-ray millisecond pulsars, as described in Chapter 2, are the most stable among all the types of pulsars. X-ray millisecond pulsars, for their extremely high stability, could ideally lead to a higher accuracy compared to normal pulsars. The possibility of spacecraft navigation using optical observations of pulsars had not been considered in any studies. The only motivation for this decision is the very low number of the pulsars for which the optical coun-

terpart is known and actually seems not to be sufficient [Deng et al., 2013]. In this thesis optical pulsars have been considered. The idea is that in the optical band the number of photons is much higher than in the X-ray band. Moreover the optical technology is much more tried and tested. Using optical pulsars, the telescope dimension and the observation time required by a pulsar navigation system would be more affordable given the higher number of photons than in the X-ray. Furthermore, there are different pulsar navigation techniques that make use of only one pulsar to correct the spacecraft position.

3.2.2 In Orbit Demonstrations

Currently, pulsars navigation systems have already been tested in orbit. In this section there are some of the important details of the in-orbit demonstrations of this system.

- *ARGOS*: was the first experiment in 1999 of the pulsar navigation, [Mitchell et al., 2015]. The test explored a broader vision of X-ray navigation and it was not limited to position determination using pulsars but also studying the use of occultations, a technique useful for satellites in orbits near planets.

- *POLAR*: is a Gamma-Ray Bursts Polarimeter which was launched in 2016 and its aim was to measure the polarization of the gamma-ray bursts. Because of its large effective area, of about 200 cm^2, and FOV (Field of View), of about 2π Sr, the instrument could be used to detect photons from pulsars and it could be used for testing pulsar navigation, [Zheng et al., 2017]. The instrument observed the Crab pulsar for 31 days and the orbit was determined with an orbit deviation within 20 km, testing a new navigation method *SEPO* (Significance Enhancement of Pulse-profile).

- *NICER*: is composed of 56 identical X-ray telescopes (effective area of about 2000 cm^2). The instrument was launched on the ISS in 2017. It measured the signals of five millisecond pulsars determining the position within 5 km.

- *Insight-HXMT*: is a telescope satellite launched in 2017 and which is composed of three X-ray telescopes (effective area of about 5000 cm^2). Using five-day long observation of the Crab pulsar and the SEPO method, the position and the velocity of the satellite were determined within 10 km and 10 ms^{-1}, respectively [Zheng et al., 2019].

3.2.3 Problems with the Pulsar Navigation

The problems related to pulsar navigation are listed in this section. These can be divided into two categories: on the one hand there are problems related to the nature of the pulsars and on the other problems related to the instrumentation needed for efficient satellite navigation. In order to understand clearly the problems with each pulsar navigation technique it is useful to know the different methods that can be used (the methods will be fully described later in the thesis).

Pulsar stars emits radiation with very stable period, which steadily increases as the pulsar releases its rotational energy. However, as seen in Chapter 2, these sources show different type of irregularities. The average pulse shape is stable and characteristic of each pulsar, but the irregularities determine the accuracy of the navigation system. For this reason it is essential to understand what are the consequences of signal irregularities. Pulsars rotation is due to natural phenomena, this leads to irregularities of the detected signal. As discussed in Section 2.2, pulsars present two types of irregularities: glitches and timing noise.
Typically *glitches* are shown by the younger pulsars and they are difficult to model, hence to predict. To solve this problem the only thing to do is to update as much as possible the ephemeris of each pulsar used in the navigation system. Another way to partly bypass the problem is to use millisecond pulsars that are more stable compared to normal pulsars.
The *timing noise* has a great influence on the accuracy of the position determination of the spacecraft. This noise has two components: white noise and red noise. White noise can be eliminated increasing the statistics, hence increasing the observation time. Red noise is difficult to eliminate but it can be reduced with an accurate study of the prediction of the spin evolution of pulsars. Furthermore, the red noise is only important in long-term observation of the pulsar.
The periodic nature of the pulsars signal leads to an *ambiguity problem* on the determination of the spacecraft. The unknown is the integer number of pulses in the detection between the pulsar and the spacecraft. The computational cost to solve this problem is extremely high if the absolute position of the spacecraft needs to be determined, but it is smaller if the initial guest on the position of the spacecraft is close to the real position. In pulsar navigation there exists techniques that offer the possibility to navigate both with no a-priori position information and with a-priori estimate of the position as will be discussed later in the thesis. However, different methods were suggested to improve the performance in the case of absolute position determination constraining the integer number of pulses in the navigation solution.
Another problem with the pulsars navigation system is the fact that the system is not completely autonomous. In fact to reconstruct the template of the signal in a reference frame the *ephemeris* (frequency and first derivative of the frequency) are necessary. As specified previously in this section, it is useful to update the ephemeris as much as possible, to compute the position determination with high accuracy. All this means that observation time from ground and space telescopes is required. The work that a navigation system would require is something like the Jodrell Bank Observatory[1] does for the Crab pulsar [Lyne et al., 1993]. The Jodrell Bank Observatory hosts a number of radio telescopes that are part of the Jodrell Bank Centre for Astrophysics at the University of Manchester. The ephemeris are updated almost monthly only for the Crab pulsar, but a navigation system that will use different pulsars will need, at least monthly ephemeris for all the pulsars used.
A practical problem is in the *instrumentation* that a spacecraft will need to have on board. Some of the techniques involve the observation of 3 or 4 pulsars simultaneously. This implies the need for complex instrumentation, even with multiple mobile telescopes. Furthermore, the dimensions of the telescopes need to be investigated.

[1] http://www.jb.man.ac.uk/ pulsar/crab.html

The signal, specially for the optical band, is weak so in order to reach a high SNR (Signal to Noise Ratio) a large telescope is required. Nevertheless the instrumentation should be able to be installed on the satellite.

4. Pulsar Navigation Techniques

This chapter describes the theory behind optical pulsar navigation. The pulsar navigation concept and the various possible navigation techniques with the related features and problems are described. Pulsar navigation techniques can be divided according to the different types of observations that can be used. There are two main types of measurements for pulsar navigation, namely the phase measurements [Shemar et al., 2016], described in Section 4.2 and the technique that uses significance analysis of the pulse profile and orbit dynamics [Zheng et al., 2019], analyzed in Section 4.3.
Actually, other techniques could ideally be used for satellite navigation but these have not been considered because they are not suitable for pulsar navigation [Kaune, 2012]. These techniques and the reasons why they cannot be used in our system are reported in the following points:

- *Angle of Arrival* (AoA): it is the measurement of the angle of arrival of the signal which will be different depending on the position of the receiver with respect to the position of the signal source. The AoA measurement cannot be used in our case. The distance from the spacecraft to the pulsar is so much larger than the spacecraft's possible travel distance that the angle of arrival of the pulsar signals is practically constant everywhere in the solar system. If we take a typical distance of 1 kpc (kparsec)$\sim 2 \cdot 10^7$ UA between the pulsar and the SSB (Solar System Barycenter), this assumption is satisfied in all the solar system as $||x||/1\text{kpc} << 1 \rightarrow ||x|| < 1\text{kpc}/100 \approx 3 * 10^{17}$ m$\approx 2 * 10^5$ UA, where x is the vector from the SSB to the spacecraft [Sala et al., 2004]. This fact simplifies the location algorithm based on the ToA measurements, which will be described in Section 4.2.1.

- *Frequency of Arrival* (FoA): it is based on Doppler shift measurements in the arrival signal. The measured Doppler shift will be different depending on the velocity of the spacecraft with respect to the signal source. The FoA measurement cannot be used in our case. As already explained in Section 2, pulsar radiation is synchrotron radiation which is a continuum and there are not, to date, pulsars which show emission or absorption lines in their spectrum. It is not possible without spectrum lines to measure the Doppler shift.

- *Received Signal Strength* (RSS): it is based on the fact that, depending on the distance of the spacecraft from the signal's source, the received signal strength would be different. The RSS measurements cannot be used in our case, because pulsars are at such a great distance that no instrument is able to measure the

tiny difference in the strength of the received signal inside the solar system. More in details, this difference is less than the shot noise thus probably the measurement is physically impossible.

4.1 Pulsar Navigation Concept

The pulsar navigation technique is based on the use of pulsar timing information to determine position and velocity of spacecraft. One of the most important requirements is a reliable timing model for the observed pulsar. The steps to reconstruct the pulse shape from observational data have been already explained in Chapter 2. Due to the fact that the measure is the ToA of photons at the detector, it is straightforward that the measurements are closely linked with position and velocity of the detector in space. The pulse phase of a pulsar has to be modelled at an inertial reference location, inertial in the sense that it does not accelerate with respect to the pulsars. The common inertial reference system usually used is the one with origin at the center of mass of the solar system the Solar System Barycentre (SSB) and the barycentric dynamic time (TDB) as time coordinate. Actually, this reference system is quasi-inertial. Arrival times of detected photons need to be corrected

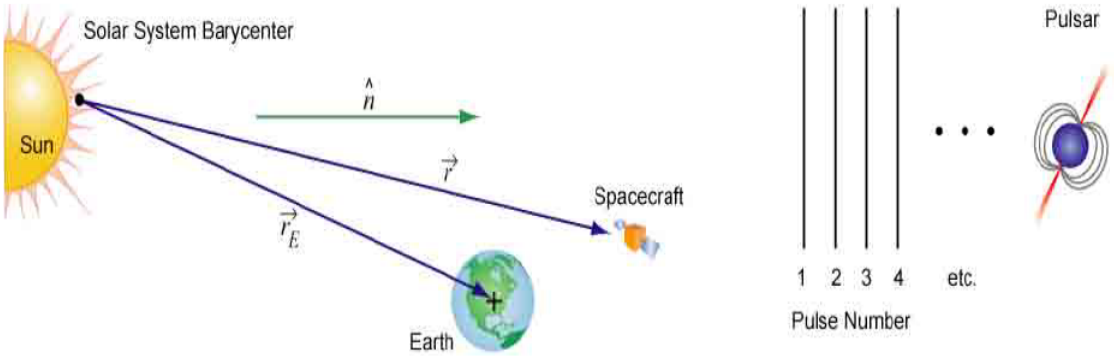

Figure 4.1: Pulsar pulse arrival times [Graven et al., 2008]. The figure shows the pulses from a pulsar as they arrive into the solar system relative to the SSB inertial frame and a spacecraft orbiting Earth. $\hat{n}$ is the unit vector from the SSB to the pulsar.

to the SSB. The time conversion of the photons is usually done with the software, *Tempo*2[1] [Hobbs et al., 2006]. *Tempo*2 is used for the analysis of pulsar pulse time of arrival for ground observation. The software accounts for the effects of a binary orbital motion, the secular motion of the pulsar or binary system, interstellar, Solar system and ionospheric dispersion, observatory motion (including Earth rotation, precession, nutation, polar motion and orbital motion), tropospheric propagation delay, and gravitational time dilation due to binary companions and Solar system bodies. The summarized transformation equation which Tempo2 software uses to convert the measured ToA to the SSB is the following:

$$\Delta t = \Delta C + \Delta A + \Delta E_{\odot} + \Delta R_{\odot} + \Delta S_{\odot} - D/f^2 + \Delta VP + \Delta B \qquad (4.1)$$

[1] http://www.atnf.csiro.au/research/pulsar/ppta/tempo2

where ΔC contains the clock corrections, ΔA the atmospheric propagation delays, $\Delta E_\odot$ the Solar System Einstein delay, $\Delta R_\odot$ the Solar System Roemer delay, $\Delta S_\odot$ the Solar System Shapiro delay, D/f^2 models the dispersive component of the light travel time, ΔVP describes the excess vacuum propagation delay due to secular motion and ΔB contains terms which describe any orbital motion.
Usually clocks such as hydrogen masers used by ground observations have a good short term stability, but on longer time scale these clocks deviate (the accuracy is of the order of 10^{-9} second per day). On Earth, it is possible to remove these errors down to the precision provided by the best terrestrial time scale. However, on a satellite, the on-board *clock* will drift over time and errors in the clock will lead to incorrect determination of the barycentric arrival times. The *atmospheric delay* does not need to be considered for a satellite navigation. *Einstein delay* quantifies the change in times due to variation in clocks due to changes in the gravitational potential of the Earth and the Earth's motion, hence this component does not need to be considered for a pulsar navigation system. *Roemer delay* is the simple vacuum delay between the arrival of the pulse at the observatory and the SSB. *Shapiro delay* is due to Solar System objects which accounts for the time delay caused by the passage of the pulse through large gravitational fields. A similar transformation needs to be done for the measured photons at the spacecraft. The *dispersive delays* need to be considered only for radio observations. The value of the delay is $\propto f^{-2}$ where f is the observational frequency that in the radio case is extremely low. *Shklovskii effect* and *radial motion* account for secular motions of the pulsar relative to the SSB. This effect is important for long-term observation hence it is not important for satellite navigation. Clearly, the software which will correct the arrival times of the photon detected at the spacecraft will be less complex than *Tempo*2 software. In fact, this software reaches 1 ns level of precision which is more than what is necessary for a navigation system as will be shown later in the document. We remark that in this thesis there is not the description of a possible navigation software. In fact, the aim is only to study feasibility and achievable accuracies of a navigation system with optical pulsars. In any case, in other studies a time conversion equation for a pulsar navigation system has been proposed as the following:

$$t_{b_k} = t_{obs_k} + \frac{1}{c}[\widehat{\mathbf{n}}\cdot\mathbf{r_k} - \frac{r_k^2}{2D_0} + \frac{(\widehat{\mathbf{n}}\cdot\mathbf{r_k})^2}{D_0} + \frac{\mathbf{r_k}V\Delta t_k}{D_0} - \frac{(\mathbf{r_k}V\Delta t_k)\widehat{\mathbf{n}}\cdot\mathbf{r_k}}{D_0} - \frac{(\mathbf{b_k}\cdot\mathbf{r_k})}{D_0} + \frac{(\mathbf{b_k}\cdot\mathbf{r_k})\widehat{\mathbf{n}}\cdot\mathbf{r_k}}{D_0}] + \sum_{i=2}^{PB_{SS}} \frac{2GM_i}{c^3} ln|\frac{\widehat{\mathbf{n}}\cdot\mathbf{r_{k_i}} + r_{k_i}}{\widehat{\mathbf{n}}\cdot\mathbf{b_{k_i}} + b_{k_i}} + 1|. \quad (4.2)$$

The barycentered time of k-th pulsar pulse, t_{b_k}, is converted from the receiver's observed time, t_{obs_k}, considering the various corrections. The values are defined as follows: $\widehat{\mathbf{n}}$ is the unit vector from the SSB to the pulsar; $\mathbf{r_k}$ is the spacecraft position relative to the SSB; D_0 is the distance to the pulsar at the *zero*-th pulse transmission; V is the pulsar's proper motion that is small and can be simplified; Δt_k is the difference in transmission time between the *zero*-th pulse and the k-th and $\mathbf{b_{k_i}}$ is the Sun's centre relative to the SSB origin. Such equation considers Roemer delay, Doppler effects and Shapiro delay and it was defined by Sheikh et al. [2006].

However, the purpose is to correct all the effects which introduce delays at the arrival time of the photons at the detector and return the pulse shape at the SSB. This correction requires knowledge of the detector position and velocity as input parameters. The input parameters can be assumed or deduced from a previous position determination. Another possibility is to require assistance from external sources, as for example the DSN (Deep Space Network), or, if the spacecraft is close to Earth, the GPS (Global Positioning System) or GNSS (Global Navigation Satellite System). In any case, additional autonomy can be provided if an on-board orbit propagator is implemented in the navigation system to provide a continuous estimate of the spacecraft's dynamics during pulsar observations. The position determined by the propagator can also be compared to the estimated position using pulsar navigation techniques. Comparing the position determined with the orbit propagator or the other on-board instruments, such as accelerometer or gyroscope, can be useful to calibrate them. As described in Chapter 3, the INS (Inertial Navigation System) is an autonomous navigation system in which precision diminishes with time. Errors in the measurements can be eliminated comparing the measurements with a pulsars navigation system.

The basic concept of pulsar navigation systems is the following. After the baricentrization of time of arrival of each photon the pulse profile can be reconstructed using the techniques already described in Chapter 2. If in the baricentrization the input position of the detector is affected by errors the measured pulse shape and the template will not be identical. The way the differences between the measured pulse shape and the template are measured gives origin to the different navigation techniques. By using one of all the possible navigation techniques the position of the spacecraft can be determined.
It is possible to improve the estimated position using iterated approaches. Hence the obtained pulse profile can continuously be improved during iterated observations. If position and velocity of the spacecraft are assumed but the pulse profile is not correct a better baricentrization has to be searched. The observational profile is permanently compared with a pulse profile template in order to observe and measure differences between the two. The template at the epoch of observation can be easily calculated thanks to the predictability of phase evolution of pulsars. The position of the spacecraft can be estimated only after that the template and the observational profile are in the same reference system. The way observational profile and the template are compared give rise to different techniques. The two possible pulsar navigation techniques are described in the following sections.

4.2 Phase Measurements

The basic concept of the phase measurement techniques is the comparison at the SSB of the observed pulse phase at the spacecraft with the predicted one: if the input position and velocity in the baricentrization are not correct a phase shift between the observed profile and the model will be measured (see Figure 4.2).
As previously said in Section 2.2, the pulse evolution of pulsars is predictable

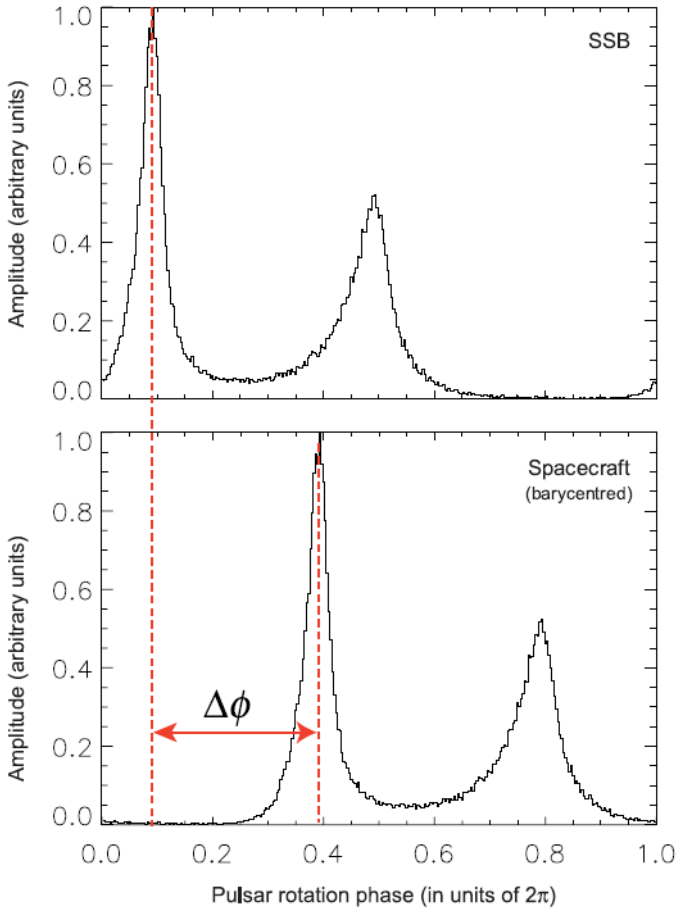

Figure 4.2: The top profile is the pulse expected at the SSB. The bottom profile is the pulse measured at the spacecraft. The assumed position is wrong if a phase shift $\Delta\phi$ between the two is observed. The measure can be made considering the phase of the peak at the SSB [Becker et al., 2013].

because of their high stabilities. The predicted pulsar signal phase at a future time t is:

$$\phi^{SSB}(t) = \phi^{SSB}(T_0) + f(t - T_0) + \sum_{m=1}^{N} \frac{f^{(m+1)}(t - T_0)^m}{(m+1)!} \tag{4.3}$$

where $\phi^{SSB}(t)$ is the predicted phase at the SSB reference, T_0 is the epoch in which the phase was known from the catalogues, f is the frequency of the pulsar and $f^{(m)}$ are its derivatives, which represent the phase changes over the time. The order of the derivative to be considered in the navigation system depends on the features of the considered pulsar and on how updated the ephemeris are. To get a precise phase evolution of the observed pulsars the ephemeris need to be updated as much as possible. As already previously said in the document, a catalogue of the pulsars ephemeris to use for possible pulsar navigation systems is needed. This catalogue would be similar to the one the Jodrell Bank observatory has for the Crab pulsar. The ephemeris of the Crab pulsar are updated almost every month. Furthermore, the ephemeris need to be communicated at the spacecraft. In this sense the navigation system is not properly an autonomous system. This fact leads to the problem that

ground observatories have to continuously observe pulsars. However, for an optical navigation system this is not a big issue because a very large telescope is not required to detect, for example, the Crab signal. Moreover, even a radio telescope can be used to get the ephemeris of the pulsars. As already mentioned in Chapter 2, radio and optical observations show a delay in time of arrival and it can be corrected. While in the case of the X-ray observation only space telescopes can be used to study the pulse shape of the pulsars that are different from optical and radio ones.
The methods which make use of phase measurements can be called Time of Arrival (ToA). The ToA method uses the predictability of the pulsar pulses and compares the detected pulses. The comparison between the two pulses is usually made at the main peak phase (see Figure 4.2): because it corresponds to the point where there is more signal and more statistics. There are two different techniques which make use of the phase measurements: delta correction and absolute navigation. Both these techniques can be used with an iteratively approach.
Figure 4.3 summarizes the position determination process. To improve the accu-

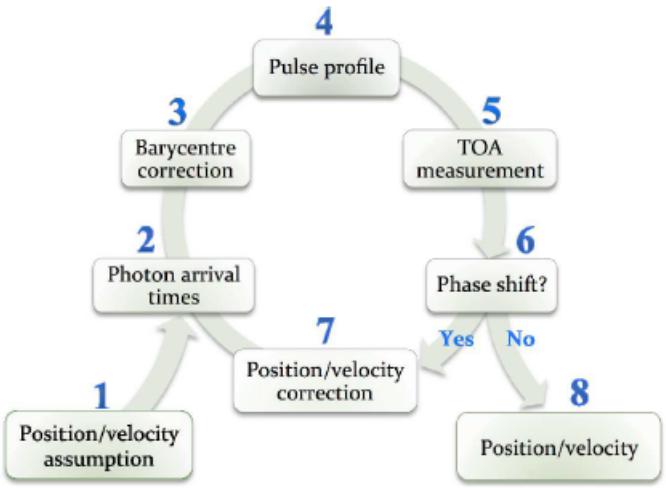

Figure 4.3: Phase measurements methods permit to measure the position of a spacecraft; they can be used with an iterative determination of position and velocity [Becker et al., 2013].

racy of the position determination the process can be done iteratively. The first step is the measure of the photons arrival times. In the baricentrization an assumption of position and velocity is required. Then, the predicted pulse profile at the epoch of observation has to be determined using the ephemeris of the used pulsar. Now the two pulses can be compared and if a phase shift is measured the position and velocity can be corrected and the process can restart implementing the new values of position and velocity in the baricentrization. The process can be repeated until no phase shift is measured.

There are different phase measurement techniques depending on how many pulsars can be observed. *Delta correction* uses only one pulsar signal measured at the spacecraft and compares it to the predicted one. The predicted pulsar pulse phase at an epoch t is computed using equation 4.3. The measured signal is the time of arrival (ToA) of the pulsar pulse. After the predicted pulse and the measured pulse

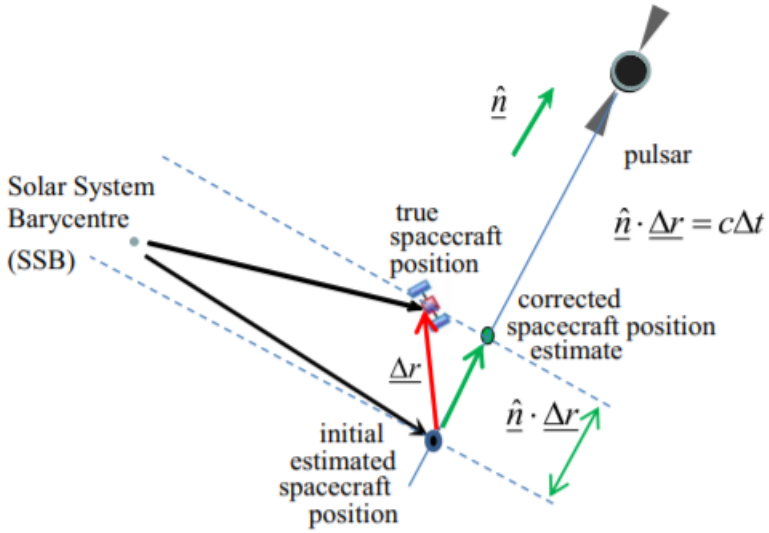

Figure 4.4: Delta correction is a method that permits the measure of the position of a spacecraft in the direction of the measured pulsar [Shemar et al., 2016].

are in the same reference frame, they can be compared and the difference gives the timing residual. This timing residual is equivalent to the light time delay between estimated and true position along the line of sight of the pulsar. Usually the measure that can be considered is the phase shift of the pulse peak, see Figure 4.2. If the input position of the spacecraft in the baricentrization is not the corrected one a phase shift of the main peak is measured. On the contrary if the phase shift is nearly zero the position and velocity used in the baricentrization are correct. In the case of Delta correction technique, the phase shift corresponds to a range difference Δx along the line of sight toward the observed pulsar defined as follow:

$$\Delta x = cP(\Delta\phi + n) \tag{4.4}$$

where c is the speed of light, P is the pulse period, $\Delta\phi$ is the measured phase shift and $n = 0, \pm1, \pm2..$ an integer number that takes into account the periodicity of the observed pulses.
Delta correction uses only one pulsar to correct the assumed position of the spacecraft. The instrumentation needed for the system is not very complex. Considering that, only one pulsar has to be observed at a time, one telescope is enough. The dimension of the telescope need to be investigated depending on what the characteristic emission of the selected pulsar is.
The achievable accuracy in the position determination of this method depends on the accuracy of the determination of the phase peak. The determination of the peak depends on the system clock errors and on pulsar timing errors. On-board clocks are usually very stable but they can drift after a long time. If the clock drift cannot be modelled it induces errors in the measurements of photons time of arrival. Pulsar timing errors are difficult to model, as previously said in Chapter 2, and they will determine the achievable accuracy of the navigation system. Later in the document this problem will be analyzed in detail.

Delta correction can be used to correct the position in one direction. It is not possible to estimate the position in three dimensions, unless measurements of different pulsars are available. The offset in three dimensions can be determined by combining measurements from different pulsars. For a three dimensions position determination at least three pulsar pulses need to be measured. By observing more than three pulsar, the clock drift of the on-board clock can be corrected. Moreover, it is possible to constrain the ambiguity problem or rather determine the integer number of pulses between the pulsar and the spacecraft. The three dimension position de-

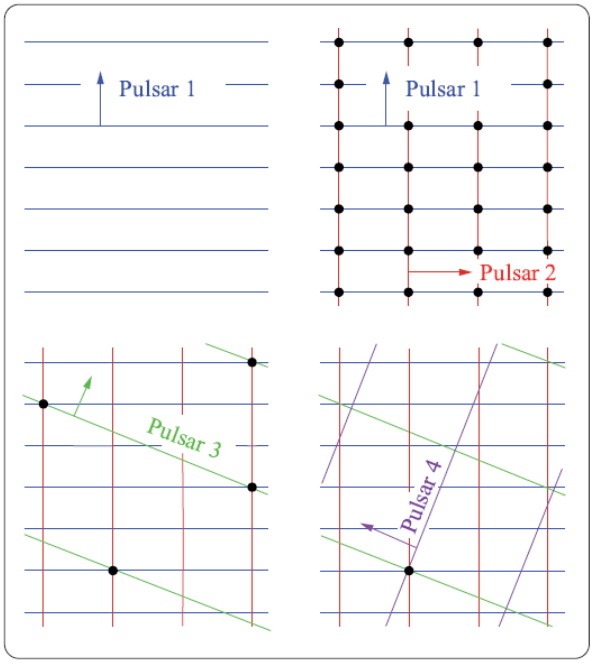

Figure 4.5: Three dimension position determination is possible observing at least three pulsars. The arrows point along the pulsar's lines of sight and the straight lines represent lines of constant pulse phase [Becker et al., 2013]. If a fourth pulsar is available the ambiguity problem could be solved.

termination technique uses the signal of three or more pulsars and compares them to the predicted ones. The method is useful when a full three dimension position determination is required. As said above, only correcting the position along the line of sight of the pulsar can be carried out by observing one pulsar and using phase measurements.

It is already clear that an a-priori estimate of position and velocity of the spacecraft is necessary. The transformation of the photon times of arrival needs the input of these parameters. This problem exists in both delta correction in one dimension and in three dimensions. This estimation can be pursued with the DSN, GPS if the spacecraft is close to Earth or with an on-board orbit propagator.
Anyway it is possible to navigate in space with pulsars even without an a-priori estimate of position and velocity. *Absolute navigation* is the method by which the position of the spacecraft is determined with no a-priori position and velocity knowledge. It can happen that the spacecraft computer needs to be reset. If this happens a-priori knowledge of the position is no longer available. Anyway, it is possible to

determine the position of the spacecraft only using simultaneous observation of pulsars. This method requires the simultaneous observation of three or four pulsars. If the estimated spacecraft position is unknown it is impossible to transform the photon times of arrival at the SSB. In fact, it is necessary to have an input position and velocity information for any timing analysis software. Hence, to determine absolute position by using only pulsar signals, multiple simultaneous pulsar observations are required. The absolute position determination requires the knowledge of which specific integer phase cycle is at a certain time. It is possible to determine the unique set of cycles which satisfies the combined information of the integer phase cycle and the line of sight of pulsar directions. In this way the absolute position relative to the SSB can be computed.
The fact that more than one pulsar needs to be observed leads to the problem that the estimated position depends on the relative position of the various sources in space. The Geometric Dilution of Precision (GDOP) is an expression of the accuracy of the estimated three dimensional position. If the navigation beacons are orthogonal each beacon is contributing maximally to the two dimensions, while if the beacons are close together the contribution to different dimensions relative to the observer are less. GDOP can influence the navigation solution. Usually, the GDOP is calculated in the covariance matrix of the estimated errors of the position solution and provides a measure on how well the set of pulsars are chosen. Considering that in the optical band the sources are really a few, this technique could not be usable for our system. Moreover, the instrumentation required for the navigation is more complex compared to the one required for Delta correction or for SEPO methods, which is described in the next section. In any case, the equations of this technique are reported in Section 4.2.1; they are useful for understanding the accuracy analysis reported in the following Chapter number 6.

4.2.1 Navigation Equations

In order to analyse the achievable accuracy in the determination of the position of an optical pulsar navigation system, it is necessary to derive the navigation equations. The accuracy analyses are reported in Chapter 6. The following analysis is similar to that carried out by Sala et al. [2004], but adapted to the optical case. The study of these equations has the sole purpose to determine the achievable accuracy of phase measurement methods. Hence, these have been useful in determining in detail what are the errors which affect the phase measurement. To determine the final navigation equations it is mandatory to study the design of the instrument and consequently the navigation method which can be utilized. In this analysis the following assumptions have been made:

- simultaneous multiple pulsars observations are possible;
- at least three optical telescopes will be available on the spacecraft;
- the ephemeris of the various selected pulsars are defined in the radio band;
- selected pulsars are sufficiently stable so that only the first order of the frequency derivative can be considered in the determination of the phase pulse

template;

- all the contributing noises are zero-mean random Gaussian.

The phase evolution of the pulsar signals at the SSB, as seen above, is defined as

$$\phi_k^{SSB}(t) = [\phi_k^{SSB}(T_0) + f_k(t - T_0) + \sum_{m=1}^{N} \frac{f_k^{(m)}(t - T_0)^m}{m!})]_w, \tag{4.5}$$

where k is the k-th pulsar and w is the phase wrapping operation defined as $0 \leq [\phi]_w = \phi + m_\phi < 1$ and with $\phi_k^{SSB}(t)$ phase at the observation time; $\phi_k^{SSB}(T_0)$ phase at a reference time T_0; $f_k = 1/T_k$ frequency of the k-th pulsar where T_k is the period of the k-th pulsar and $f_k^{(m)}$ is the m-th derivative of the frequency.
The Phase Observation of the pulsar signals at position $\mathbf{x}$ is defined as

$$\tilde{\phi_k^{\mathbf{x}}}(t) = [\phi_k^{SSB}(t - \tau_k) + w_{\phi_k}]_w = [\phi_k^{SSB}(T_0) + f_k(t - \tau_k - T_0) + w_{\phi_k}]_w, \tag{4.6}$$

where τ_k is the phase delay with respect to the SSB and w_{ϕ_k} is the additive Gaussian noise sample associated with the estimate $\tilde{\phi_k^{\mathbf{x}}}(t_0)$. It has to be noted that only two terms of the phase evolution have been used exploiting the vicinity of t to T_0. This is not a strong assumption as the rest of terms can only affect after several months, Sala et al. [2008]. The unknown specific delay for the k-th phase estimate τ_k depends linearly on the position of the spacecraft $\mathbf{x}$ and the direction of arrival for the specific pulsar at the SSB and it can be determined in the following way:

$$\tau_k = \frac{\widehat{\mathbf{u}}_\mathbf{k}^\mathbf{T} \cdot \mathbf{x}}{c}, \tag{4.7}$$

where $\widehat{\mathbf{u}}_\mathbf{k}$ is the unitary vector from the SSB to the pulsar and c is the speed of light. The delay with respect to the SSB can be understood as the projection of the position vector $\mathbf{x}$ into the constant angle of arrival of the pulsar, see Figure 4.6. If we substitute (4.7) in the equation (4.6) and exploit the wrapping operation we have:

$$\tilde{\phi_k^{\mathbf{x}}}(t) = \phi_k^{SSB}(T_0) + f_k(\Delta t_0 - \frac{\widehat{\mathbf{u}}_\mathbf{k}^\mathbf{T} \cdot \mathbf{x}}{c}) + m_k + w_{\phi_k}, \tag{4.8}$$

where $\Delta t_0 = t - T_0$ and m_k is an unknown integer related with the number of wrapped phase cycles for each pulsar signal.
Rearranging the terms of the equation (4.8) we can get the relation between measurements and unknown parameters, i.e. time, position and ambiguity:

$$y_k = f_k^{-1}(\tilde{\phi_k^{\mathbf{x}}}(t) - \phi_k^{SSB}(T_0)) + T_0 = t - \frac{\widehat{\mathbf{u}}_\mathbf{k}^\mathbf{T} \cdot \mathbf{x}}{c} + f_k^{-1} m_k + f_k^{-1} w_k; \tag{4.9}$$

where y_k are the linear transformed initial phase delays of the k-th pulsar. We need to add in this equation the correction for the dispersion measure Δt_{DM}, due to the delay induced to the light from the interstellar medium, and the correction Δt_{OR} for the delay we have when we compare the radio phase ephemeris and the optical measures. Assuming these additional factors we get:

$$y_k = f_k^{-1}(\tilde{\phi_k^{\mathbf{x}}}(t) - \phi_k^{SSB}(T_0)) + T_0 - \Delta t_{DM} - \Delta t_{OR} = t - \frac{\widehat{\mathbf{u}}_\mathbf{k}^\mathbf{T} \cdot \mathbf{x}}{c} + f_k^{-1} m_k + f_k^{-1} w_k; \tag{4.10}$$

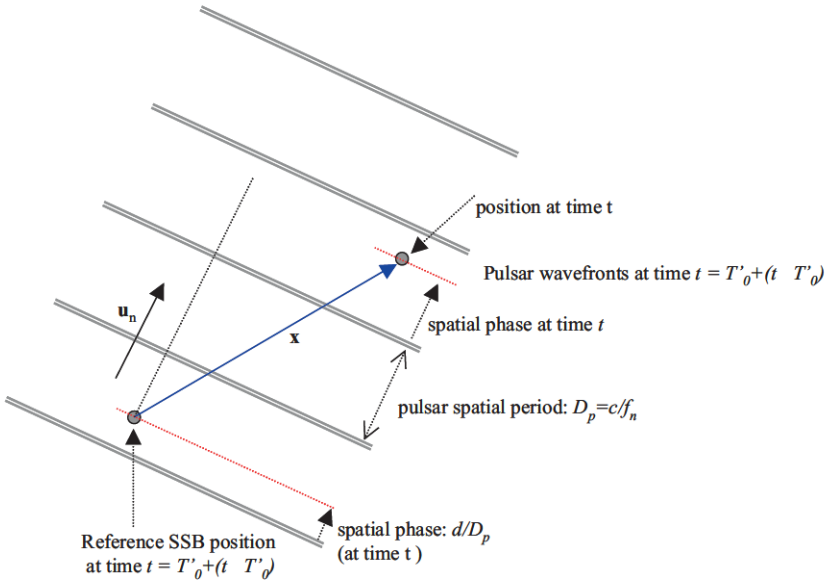

Figure 4.6: Geometrical interpretation of the phase estimate. The $\mathbf{x}$ is the unknown position of the spacecraft defined respect to the SSB. The source of ambiguity is observed as the integer number of spatial pulsar periods D_p in the direction $\mathbf{u_n}$ [Sala et al., 2004].

The dispersion measure (DM) is only important for radio observation of pulsars. In fact, the time delay due to dispersion is:

$$\Delta t_{DM} = \frac{e^2}{2\pi m_e c} \frac{DM}{f^2} \tag{4.11}$$

where in the first fraction there are the constants e electron charge, c speed of light and m_e electron mass. Then, it can be noticed that the dependence on the observation frequency is f^{-2}, and in the case of radio observation this is very low compared to the optical frequency. DM, dispersion measure, is the integrated column density of free electrons between an observer and a pulsar $DM \equiv \int_0^d n_e \, dl$. Since radio band has a very low frequency, in the presence of charged particles there is a strong electrostatic interaction between the light and the charged particles. The interaction causes a delay in the propagation of the light. As seen in equation 4.11, the delay is a function of the radio frequency and the masses of the charged particles. The more energetic the photons are the more they tend to push past the charged particles with little effect on their speed, whereas lower frequency photons are more significantly delayed. Δt_{OR} correction has to be considered if the ephemeris are in the radio band. As seen in Section 2.2, there is a delay in the time of arrival between optical and radio band. If the ephemeris are known in optical wavelength this contribution does not need to be counted.
Finally, we can express the equations for the ToA method in vector notation as

follows:

$$\begin{bmatrix} y_1 \\ \vdots \\ y_k \end{bmatrix} = \begin{bmatrix} \mathbf{1}_k \begin{bmatrix} -\frac{\hat{\mathbf{u}}_1^{\mathbf{T}}}{c} \\ \vdots \\ -\frac{\hat{\mathbf{u}}_k^{\mathbf{T}}}{c} \end{bmatrix} \end{bmatrix} \begin{bmatrix} t \\ \mathbf{x} \end{bmatrix} + \begin{bmatrix} f_1^{-1} & 0 & 0 \\ 0 & \ddots & 0 \\ 0 & 0 & f_k^{-1} \end{bmatrix} \begin{bmatrix} m_1 \\ \vdots \\ m_k \end{bmatrix} + \begin{bmatrix} f_1^{-1} & 0 & 0 \\ 0 & \ddots & 0 \\ 0 & 0 & f_k^{-1} \end{bmatrix} \begin{bmatrix} w_{\phi_1} \\ \vdots \\ w_{\phi_k} \end{bmatrix} \tag{4.12}$$

We can rewrite the final model for the phase estimates as:

$$y = \begin{bmatrix} \mathbf{1_k} & -\mathbf{U} \end{bmatrix} \begin{bmatrix} t \\ \mathbf{x} \end{bmatrix} + \mathbf{F}\mathbf{m} + \mathbf{w_y}; \tag{4.13}$$

where $\mathbf{U}$, $\mathbf{F}$ and $\mathbf{w}$ are defined as:

$$\mathbf{U} = \begin{bmatrix} -\frac{\hat{u}_1^T}{c} \\ \vdots \\ -\frac{\hat{u}_k^T}{c} \end{bmatrix}; \mathbf{F} = \begin{bmatrix} f_1^{-1} & 0 & 0 \\ 0 & \ddots & 0 \\ 0 & 0 & f_k^{-1} \end{bmatrix}; \mathbf{w_y} = \mathbf{F} \begin{bmatrix} w_{\phi_1} \\ \vdots \\ w_{\phi_k} \end{bmatrix}. \tag{4.14}$$

Under the assumption that the noises are all zero-mean random Gaussian, e.g. $\mathbf{w_y} \sim N(0, R_y)$, we can write the covariance matrix R_y. This matrix will be the sum of all the covariance matrices of all the noise contributions, e.g. the measured phase at the position x , the variance of the determination of the model phase at the SSB, the variance of the dilution measure and the variance due to comparing the optical data with the radio ones. The covariance matrix of ϕ^x is defined as follows:

$$\mathbf{R}_{\phi^{\mathbf{x}}} = E[\mathbf{w}_{\phi^{\mathbf{x}}} \mathbf{w}_{\phi^{\mathbf{x}}}^{\mathbf{T}}] = \mathbf{F}\mathbf{R}_{\phi}\mathbf{F}^{\mathbf{T}} = \begin{bmatrix} f_1^{-2}\sigma_{\phi_1^x}^2 & 0 & 0 \\ 0 & \ddots & 0 \\ 0 & 0 & f_k^{-2}\sigma_{\phi_k^x}^2 \end{bmatrix}; \tag{4.15}$$

This component of the covariance matrix depends on the area of the on-board telescope, the kind of detector and the noise of the background of the pulsar and the dark counts of the detector. Moreover, we have to consider the uncertainties of the spacecraft clock for the determination of the time of arrival of the pulsar's signal.
The covariance matrix of ϕ^{SSB} is defined as follows:

$$\mathbf{R}_{\phi^{\mathbf{SSB}}} = E[\mathbf{w}_{\phi^{\mathbf{SSB}}} \mathbf{w}_{\phi^{\mathbf{SSB}}}^{\mathbf{T}}] = \mathbf{F}\mathbf{R}_{\phi}\mathbf{F}^{\mathbf{T}} = \begin{bmatrix} f_1^{-2}\sigma_{\phi_1^{SSB}}^2 & 0 & 0 \\ 0 & \ddots & 0 \\ 0 & 0 & f_k^{-2}\sigma_{\phi_k^{SSB}}^2 \end{bmatrix} \tag{4.16}$$

This component depends on how accurate the template is which we have for the k-th pulsar. We can find this information on the catalogue "Jodrell Bank Crab pulsar Ephemeris". Here, the ephemeris of the Crab Pulsar are reported monthly with the RMS of the measure.
The covariance matrix of Δt_{DM} is defined as follows:

$$\mathbf{R_{DM}} = \begin{bmatrix} \sigma_{DM_1}^2 & 0 & 0 \\ 0 & \ddots & 0 \\ 0 & 0 & \sigma_{DM_k}^2 \end{bmatrix} \tag{4.17}$$

This component depends on how accurate the estimation of the dilution measure due to the interstellar medium is. After propagating through the interstellar medium the light experiences a frequency dependent time delay that we need to take into account.
The covariance matrix of Δt_{OR} is defined as follows:

$$\mathbf{R_{OR}} = \begin{bmatrix} \sigma^2_{OR_1} & 0 & 0 \\ 0 & \ddots & 0 \\ 0 & 0 & \sigma^2_{OR_k} \end{bmatrix} \tag{4.18}$$

This component is due to the fact that the ephemeris that we have are in the radio band and there is a difference on the time of arrival between the two different observation bands. The optical peak leads the radio one and this can be caused by a different position of the two emitting regions.
At the end summing all these contributions we can derive the covariance matrix of the measurements y_k:

$$\mathbf{R_y} = \mathbf{F}\mathbf{R}_{\phi^{\mathbf{x}}}\mathbf{F^T} + \mathbf{F}\mathbf{R}_{\phi^{\mathbf{SSB}}}\mathbf{F^T} + \mathbf{R_{DM}} + \mathbf{R_{OR}} = \begin{bmatrix} \sigma^2_{y_1} & 0 & 0 \\ 0 & \ddots & 0 \\ 0 & 0 & \sigma^2_{y_k} \end{bmatrix}. \tag{4.19}$$

The covariance matrix of the method is essential to determine the accuracy of the determination of the position. In the next Chapter this matrix will be necessary for the accuracy analysis.

The following equations show that there is a linear dependence between the phase difference of the drift in the phase measure of two sequential observations and the velocity of the spacecraft. This measure can be called *Drift-ToA*.
The derivative of the phase evolution equation, equation (4.5), of the k-pulsar at the SSB is defined as

$$\varphi_k^{SSB}(t) = \dot{\phi}_k^{SSB}(t) = [f_k \dot{\Delta} t_0] \tag{4.20}$$

The derivative of phase observation of the k-pulsar at position $\mathbf{x}$ is defined as

$$\tilde{\varphi_k^{\mathbf{x}}}(t) = \dot{\phi}_k^{SSB}(t - \tau_k) = [f_k(\dot{\Delta} t_0 - \frac{\widehat{u}_k^T \dot{\mathbf{x}}}{c})) + w_{y_{D-ToA,k}}]. \tag{4.21}$$

Similar to how it was carried out previously, by rearranging the terms of these two equations (4.20) and (4.21) and applying the wrapping operation we can get the relation between the Drift-ToA measurements and the unknown parameters or rather the position derivative:

$$y_{D-ToA,k} = f_k^{-1}(\tilde{\varphi_k^{\mathbf{x}}}(t) - \varphi_k^{SSB}(T_0)) = -\frac{\widehat{u}_k^T \dot{\mathbf{x}}}{c} + f_k^{-1} w_{y_{D-ToA,k}}. \tag{4.22}$$

It must be noted that by making the derivative of the phase observation the dependence on m_k, number of phase-cycles unknown, is eliminated.
Finally, the vectors and the matrix involved can be defined as follows:

$$y_{D-ToA} = -\mathbf{U}\dot{\mathbf{x}} + \mathbf{F}\mathbf{w}_{\mathbf{y}\,D-ToA}; \tag{4.23}$$

where $\mathbf{U}$ and $\mathbf{F}$ are already defined above, $\dot{\mathbf{x}}$ is the velocity vector of the spacecraft that is the unknown parameter and $\mathbf{w}_{y_{D-ToA}} = [w_{y_{D-ToA,1}}, \ldots, w_{y_{D-ToA,k}}]$ is the vector of the zero mean Gaussian noise associated with each k-th pulsar. The noise term is considered component independent and its covariance matrix is:

$$\mathbf{R}_{\mathbf{y_D-ToA}} = E[\mathbf{w}_{\mathbf{y_D-ToA}} \mathbf{w}^{\mathbf{T}}_{\mathbf{y_D-ToA}}] = \begin{bmatrix} \sigma^2_{y_{D-ToA,1}} & 0 & 0 \\ 0 & \ddots & 0 \\ 0 & 0 & \sigma^2_{y_{D-ToA,k}} \end{bmatrix}. \tag{4.24}$$

The covariance matrix of the method is essential to determine the accuracy of the determination of the velocity. In the next Chapter this matrix will be necessary for the accuracy analysis.

4.3 Significance Analysis

SEPO (Significance Enhancement of Pulse-profile with Orbit-dynamics) is a pulsars navigation method that can determine the orbital parameters of the spacecraft using only one pulsar. The basic concept of this method is very simple compared to the idea of the phase measurement techniques. The observed pulse profile, obtained, as described above, after the time conversion to the SSB will be deformed due to the input orbit errors resulting in a decrease of the significance of the profile signal, see Figure 4.7. SEPO method, however, has not been proven mathematically. Zheng et al. [2019] performed some simulations to show that the method works with different pulse profiles.

The basic assumption with this technique is that an estimate position as input before the position determination is mandatory. The process that allows to pass from the measurement on the detector to the light curve is complex, as already said above. The measurement is the time of arrival at the detector of the photons. Then, the photons have to be converted at the SSB. The time correction at the SSB of the time of arrival of each photon is closely related with the input position of the spacecraft. If the orbit deviates from the correct position the calculated profile will be deformed from the standard profile due to the wrong phase. In Figure 4.7, the differences between the correct pulse shape and the calculated wrong pulse shape are displayed.

Implementation of the significance (or χ^2 test analysis) is any statistical hypothesis test where the sampling distribution of the test statistic in a χ^2 distribution for example can be used to test the goodness of fit. In our case the significance of the pulse profile is defined as:

$$\chi^2 = \sum_{i=1}^{N} \frac{(P(\phi_i) - \tilde{P})^2}{\tilde{P}} \tag{4.25}$$

where $P(\phi_i)$ is the counts of the profile at ϕ_i, $\tilde{P}$ is the mean counts of the profile and N is the total bin number of the profile. The significance of the calculated profile

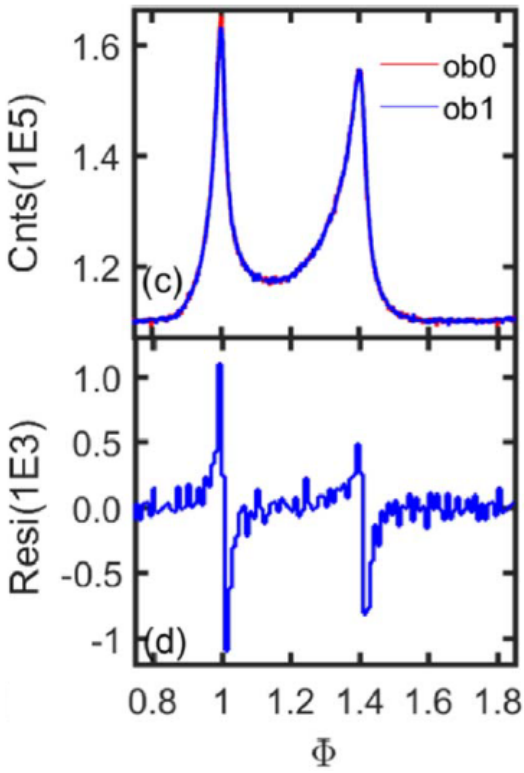

Figure 4.7: In the top figure the distortion of the pulse profile induced by changes of the initial elements can be observed. The red line ("ob0") represents the standard profile, and the blue line represents the distorted profile. The distortion is generated by errors in the input parameters. The bottom figure shows differences between the standard and distorted profile.

is expected to vary with spacecraft orbit deviation. The value of χ^2 will reach the maximum for the zero deviation, hence the true position and velocity. The more the orbit deviates from the true orbit the more the profile will be deformed and the less the value of significance.
This method uses the observation of only one pulsar to adjust the orbit parameters. The orbit elements are: eccentricity, semimajor axis, inclination angle, right ascension of the ascending node, argument of perigee and mean anomaly. Passing from orbit elements to coordinates using transformation matrices is possible. The significance analysis has to be used iteratively in order to determine the maximum value of χ^2. The processing flow of the technique is reported in Figure 4.8. The orbit forecast model is determined using orbit dynamics. The method to determine the orbital parameters will depend on the conditions of the spacecraft and the mission. In this thesis we do not go into details on this step. The orbit parameters will be affected by errors, and this leads to the possibility of defining different possible positions of the spacecraft. After the determination of the predicted orbits, the photons arrival times are corrected to the SSB and are folded to generate the predicted profiles, as previously explained. The pulsar profile template can be generated using phases

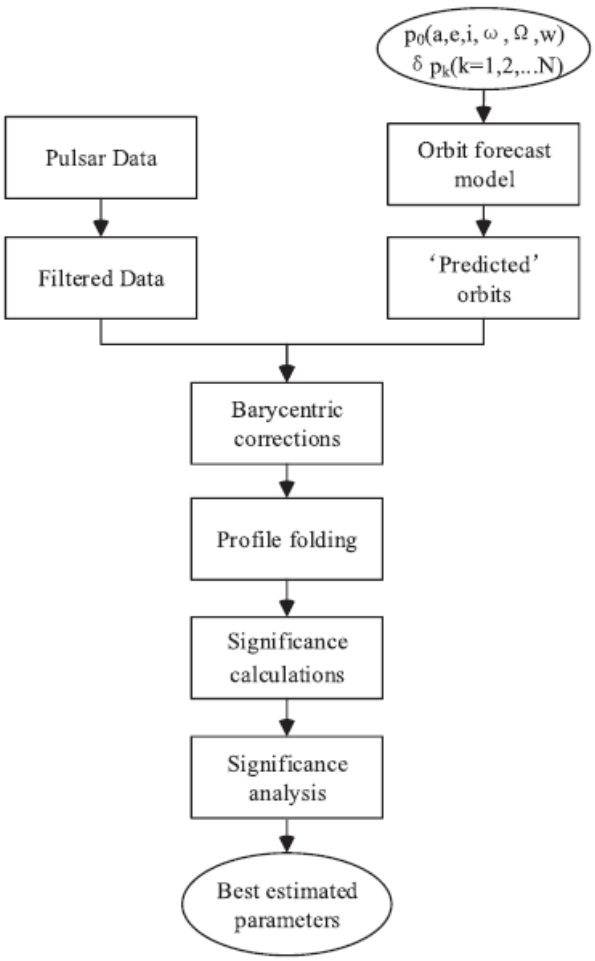

Figure 4.8: Processing flow of SEPO pulsar navigation method. The process can be used with an iteratively approach, thanks to the long-term stability characteristics of the profile, to continuously update the orbital parameters.

calculated with the phase evolution equation:

$$\phi^{SSB}(t) = \phi^{SSB}(T_0) + f(t - T_0) + \sum_{m=1}^{N} \frac{f^{(m+1)}(t - T_0)^m}{(m+1)!}. \tag{4.26}$$

In this equation, already seen above, only the first order derivative can be considered because the other orders become important only after several months (this fact will be provided in the following chapters).
At this point it is possible to calculate all the significance values for all the predicted profiles. The significance analysis consists in determining which of the predicted profiles gives the maximum value of χ^2. To determine the accuracy of the method a Gaussian function can be used. The trend between the significance of profiles and the orbit parameters is fitted with the Gaussian function and the optimal orbit parameters and the related errors are obtained. The optimal values for the six orbital parameters are determined separately. One parameter is free and the other five fixed. The method has been used in *Insight-HXMT* satellite using X-ray data of the Crab pulsar, as mentioned in Section 3.2.2. This method is new compared to the phase measurement methods which have been proposed by different papers. SEPO has

been proposed for the first time by Zheng et al. [2017] considering X-ray pulsars. The positive aspect of this technique is that one single pulsar needs to be observed to determine the orbital elements correction. This means that the required navigation system instrumentation is not complex, but only one telescope is required. However, the main problem related with this technique is the long observation time required to get high value of χ^2. In this thesis we propose the same method of Zheng et al. [2019] but considering optical pulsars. The details of our analysis will be described later in the document. In any case, our idea is that we can be competitive by observing in the optical band. In this sense, the required observation time to determine the position using optical band compared to X-ray will be less, due to the large amount of photons.

5. Selection of Optical Pulsars

In addition to possible pulsar navigation techniques it is necessary to define the possible optical pulsars usable by navigation systems. In this chapter all the known optical pulsars are reported with their light curves and features. The optical instrumentation used for studying optical timing of pulsars is described in order to understand what a navigation system, which uses optical pulsars, needs to determine its position in space. The real data used in this thesis are obtained with the Aqueye+ instrument, mounted at the Copernicus telescope in Asiago [Naletto et al., 2013], [Zampieri et al., 2015]. Moreover, a preliminary study of the accuracy of the phase measurement of the Crab pulsar, the optical pulsars distribution and an example of visibility analysis are reported and commented.

5.1 Instrumentation for Optical Photometry

Pulsar navigation systems consider pulsars as natural navigation beacons. All the studies to date performed on pulsar navigation systems focussed on X-ray pulsars as the only usable type of pulsars. The reason for this choice is the low number of pulsars in which optical pulsations are detected. The number of pulsars known to date is approximately 2000 and of these only about 1% have a known optical counterparts [Leeb et al., 2015]. There are about six rotation-powered pulsars which are suitable for navigation systems [Mignani et al., 2000]. Other optical counterparts of pulsars could still be discovered, as PSR $J1023+0038$ in which pulsations have been recently detected by Ambrosino et al. [2017] and Zampieri et al. [2019a].

From a scientific point of view multi-wavelength observations are useful to understand the physics of the emission processes of neutron stars. A particular kind of instrumentation has been developed in order to perform very fast photometry in the optical band. *Aqueye+ and Iqueye*[1], the Asiago quantum eye and Italian quantum eye, are very high speed photon counters with the capability of time tagging the detected photons with sub-ns time accuracy, developed at the University of Padova and the INAF Astronomical Observatory of Padova [Barbieri et al., 2009], [Naletto et al., 2009] [Naletto et al., 2013]. The instruments are based on single photon avalanche photo-diodes (SPADs). Aqueye+ is regularly mounted on the 1.8 m Copernicus telescope in Asiago while Iqueye was mounted on the NTT telescope in Chile and on the WHT and TNG telescopes on the Roque in La Palma. The instruments are mainly used for optical timing of pulsars, the follow-up of optical transients, and lunar and

[1] https://web.oapd.inaf.it/zampieri/aqueye-iqueye/index.html

Trans Neptunian objects occultations [Zampieri et al., 2019b].

In order to navigate in space with pulsars we need to get the pulse profile of the pulsar as already explained in Chapter 2. In the following we will consider observations performed with accurate fast photon counters, namely Aqueye+. Aqueye+, mounted on the Copernicus telescope, can record and store arrival times of all detected photons with an absolute precision better than 500 ps for hour-long observing sessions [Naletto et al., 2013]; [Zampieri et al., 2015]. To achieve high time accuracy this instrumentation makes use of a specific type of detector that allows photon counting with high absolute precision, a *SPAD* detector, (see Figure 5.1). This sin-

Figure 5.1: Picture of a MPD SPAD detector taken from: http://www.micro-photon-devices.com.

gle photon-counter is based on avalanche photo-diodes operating in Geiger mode. A satellite navigation system that will use optical pulsars as navigation beacons will need a single photon counting detector like this. To our knowledge, there is not, at this time, a space-qualified instrument of this type. Space-qualification is the process of reliability which ensures space worthiness of each component of a space instrument. The interest on space qualification of single photon counting detectors exists for other purposes; for example for Lidar, quantum communication and flight formation. Several tests have already been carried out. For example, Marisaldi et al. [2011], performed bulk damage and total dose radiation tests with protons and gamma-rays in order to evaluate the radiation hardness properties and suitability for space applications of a SPAD detector. In this sense, more effort will need to be made to develop an optical navigation system based on SPAD detectors.

5.2 Optical Pulsars

In this section all the optical pulsars known to date are described and their properties summarized.
The *ATNF*[2] radio pulsars catalogue counts more than 2600 pulsars. The *3FGL* gamma-ray pulsars catalogue counts about one hundred pulsars. On the other hand, only about ten pulsars have optical counterparts. They are listed in Table 5.1. The

[2]http://www.atnf.csiro.au/research/pulsar/psrcat

possible candidate pulsars for a navigation system are the first six in Table 5.1, e.g. those for which optical pulses have been detected. They are also those with brighter counterparts. For all of them a timing solution is available. They are: *Crab*, *Vela*, *Geminga*, PSR $B0540-69$, PSR $B0656+14$ and PSR $J1023+0038$. The magnitude are reported in Table 5.1. The first six have higher magnitude compared to the last ones.

Name	Period (s)	Period Derivative	V (mag)	Galactic Longitude (deg)	Galactic Latitude (deg)	Distance (kpc)
B0531+21 (Crab)	0.033	4.21E-13	16.6	184.558	-5.784	1.73
B0833-45 (Vela)	0.089	1.25E-13	23.6	263.552	-2.787	0.23
B0540-69	0.051	4.79E-13	22.0	279.717	-31.516	49.4
B0656+14	0.385	5.49E-14	25	201.108	8.258	0.29
J0633+1746 (Geminga)	0.237	1.09E-14	25.5	195.134	4.266	0.07
J1023+0038	0.002	6.93E-21	/	243.490	45.782	1.37
B1509-58	0.089	1.25E-13	25.7^R	320.321	-1.162	4.18
B1133+16	1.188	3.73E-15	28	241.895	69.196	0.35
B1055-52	0.197	5.83E-15	24.9^U	285.984	6.649	0.72
B1929+10	0.151	1.53E-12	25.6^U	47.382	-3.884	0.33
B0950+08	0.226	1.16E-15	27.1	228.908	43.697	0.26
J0108-1431	0.807	7.70E-17	26.4^U	140.930	-76.815	0.2
J0437-4715	0.006	5.73E-20	/	-41.963	253.394	0.14

Table 5.1: List of pulsars with optical counterparts: the first six pulsars are the ones with detected optical pulsations and for which timing data exist. The data are taken from Mignani et al. [2000] and from ATNF catalogue.

Any of the possible pulsar navigation techniques needs the knowledge of the spin frequency in order to define the pulsar template at the SSB. In order to be able to select the best candidates as natural navigation beacons it is important to understand the properties of the single optical pulsars.
The most important property for a pulsar navigation system is detectability. Pulsars are the result of supernova explosions during which the bulk of their progenitor star is expelled into the interstellar medium. The nebula of the pulsars gives an important contribution to the emitted flux, which is not negligible and it has to be taken into account as nebular background. In fact, the pulsed radiation is only a fraction of all the emitted radiation. One of the difficulties in the signal detection of the pulsars is the presence of the nebula, which drastically reduces the contrast. Not all the optical pulsars reported in table 5.1 have the nebula. The presence of the nebula is important for example for the Vela pulsar while it is not so important for PSR B0540-69.
In order to determine the shape of the pulsation it is necessary to sample it using several bins. The bin duration is constrained by the time resolution of the instrument. The second constraint comes from the fact that each bin should have enough

counts for a significant signal above the background, which implies that smaller bins require longer exposure times. For the X-ray band this fact is more binding than for the optical band in which photons are more numerous. Another important property is the stability factor. As already explained, pulsars are like a very precise atomic clock at first approximation, but actually they show timing noise. The best pulsars for a pulsar navigation system would be the type of pulsars called millisecond pulsars. This kind of pulsars shows a small spin period, $P < 20$ ms, and high rotational stability with $dP/dt \simeq 10^{-18} - 10^{-21}$ s/s. Unfortunately, only one millisecond pulsar has detectable pulsations in the optical PSR $J1023 + 0038$ [Ambrosino et al., 2017]; [Zampieri et al., 2019a]. Moreover, it is not the best candidate because it is a recycled pulsar and it shows several irregularities which are difficult to model. So, for an optical pulsar navigation system no millisecond pulsars are suitable targets. Instead, we can search among the available isolated optical pulsars for those with a sufficiently high signal that a short observation time is enough to obtain a sufficiently accurate pulse shape. If the observation time is sufficiently short, timing irregularities would be low enough not to affect the measurement. In fact, timing noise affects timing accuracy after several days [Čadež et al., 2016]. It is important to emphasize that for the phase measurement method the important factor is the accuracy of the peak phase determination. While for the SEPO method the most important factor is the high statistics of the signal.

The relevant properties of the main optical pulsars are summarized below

- PSR $B0531 + 21$ $(Crab)$: it is the brightest optical pulsar ($V = 16.6$ mag). It shows a double peak pulse profile, see Figure 5.2. The pulsar in the Crab nebula was the first pulsating source in the optical band to be detected [Cocke et al., 1969]. It is one of the most targeted objects at all wavelengths from the radio to very high energy gamma-rays. It is the test-bed for pulsars theories. In the optical band many studies, including phase analysis, have been carried out for this source. It has been found that the optical pulse leads the radio

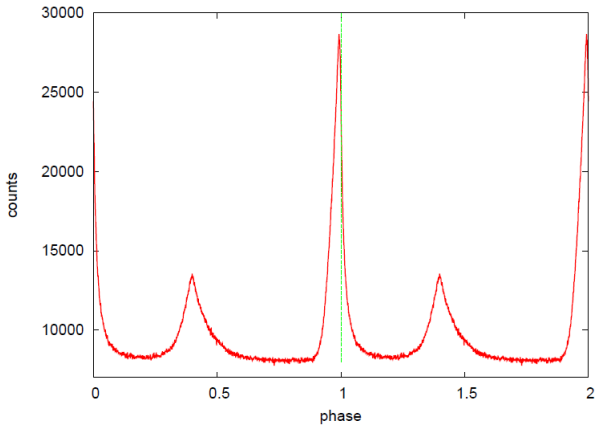

Figure 5.2: Crab pulse shape. The light curve is shown over two cycles for clarity. The vertical dashed line correspond to the position of the main peak in the radio band [Germanà et al., 2012].

one by $\sim 150 - 250\mu s$ [Zampieri et al., 2014]. The optical timing solution was

derived with an accuracy of $\sim 30\mu s$ by Germanà et al. [2012] and Zampieri et al. [2014].

- PRS $J1023 + 0038$: it is the only millisecond pulsar with detected optical pulsations [Ambrosino et al., 2017]. This pulsar is a fast spinning, weakly magnetized neutron star, called transitional millisecond pulsar (see Papitto et al. [2019] and reference therein). At the beginning it was classified as a Cataclysmic Variable. Subsequent observations showed, instead, that the source was a radio pulsar with a rotational period of 1.69 ms orbiting a $\sim 0.2 M_{\odot}$ companion with a period of 4.75 hours. This kind of sources can swing between a rotation-powered millisecond pulsar phase and an accretion phase. The neutron stars in them are believed to be recycled pulsars: old, low magnetic field pulsars re-accelerated through mass and angular momentum transfer from a companion star. Zampieri et al. [2019a] observed the pulsar for a few nights and night-to-night variations of the pulse shape were detected with the second peak varying significantly compared to the first peak. Figure 5.3 shows the pulse shape of the pulsar. The rotational period is in agreement with the value

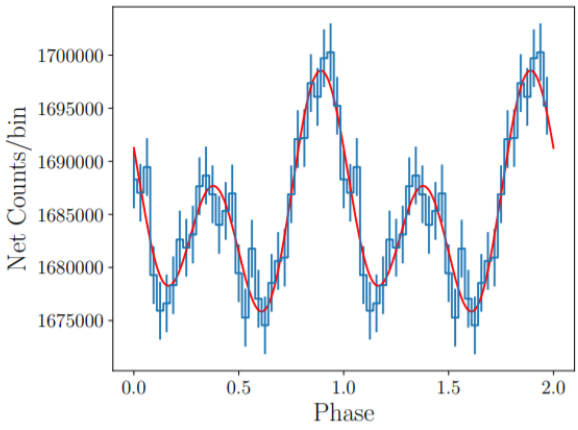

Figure 5.3: PSR J1023+0038: pulse shape. The light curve is shown over two cycles for clarity. This is the overall Aqueye+ light curve of the 2018 January observations [Zampieri et al., 2019a].

from the X-ray ephemeris, while the phase of the ascending node is shifted by $11.55 \pm 0.08s$ from the value predicted using the orbital period from the X-rays. The optical timing solution was derived with an accuracy of $\sim 12\mu s$ by Zampieri et al. [2019a].

- PSR $B0540-69$: it is the second brightest pulsar in the visible band ($V = 22.0$ mag) after the Crab pulsar [Gradari et al., 2010]. It is located in the Tarantula nebula of the Large Magellanic Cloud. The optical light curve shows a double structure in the main peak with a rising edge steeper than the trailing edge (see Figure 5.4). The period of the pulsar is 50 ms. PSR $B0540 - 69$ is the only extragalactic optical pulsar. In fact, it is located in the Large Magellanic Cloud (the distance is 49.4 kpc, see Table 5.1).

- PSR $B0833-45$ ($Vela$): it is one of the most intense sources in the gamma-ray and radio band, while it is much weaker in the optical band ($V = 23.6$ mag)

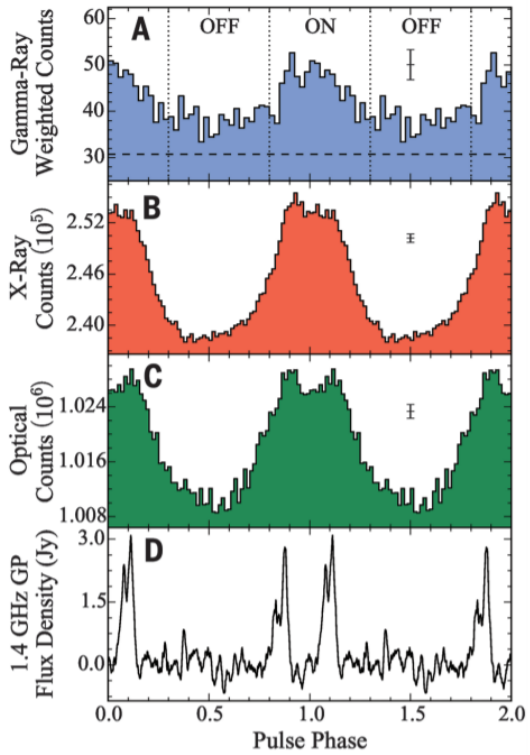

Figure 5.4: PSR $B0540-69$: pulse shape. The light curve is shown over two cycles for clarity and the optical profile corresponds to the one marked with letter **C**. This is the overall Iqueye light curve of the 2009 January and December observations obtained with NTT telescope [Fermi LAT Collaboration et al., 2015].

[Spolon et al., 2019]. It is located in the Vela nebula. The gamma and X-ray pulse profiles are very different from those in the radio and optical bands. It shows a period of 89 ms.

- PSR $B0656+14$: it is a faint optical pulsar ($V = 25$ mag) with a period of 385 ms. The first possible optical counterpart was detected by Caraveo et al. [1994], then confirmed in 1997 with HST (Hubble Space Telescope) observations. The pulse profile is double peaked with a bridge of emission between the two peaks, see Figure 5.6.

- PSR $J0633+1746$ (*Geminga*): it is one of the brightest gamma-ray sources but shows a very weak optical emission ($V = 25.5$ mag) [Mignani et al., 1994]. It has a rotational period of 0.0002 s.

The description of the various main optical pulsars is useful to understand what are the best candidates for an optical pulsar navigation system. As already mentioned, for an X-ray navigation system the best type of pulsars are the millisecond pulsars, because of their significant stability. In the optical band the situation is different. At this wavelength the count rate is much higher. Our idea is that, in order to obtain an accurate enough measurement of the pulse shape the integration time can be sufficiently short that the timing noise cannot affect the measurement. Consequently, it is possible to adopt a different type of pulsar.

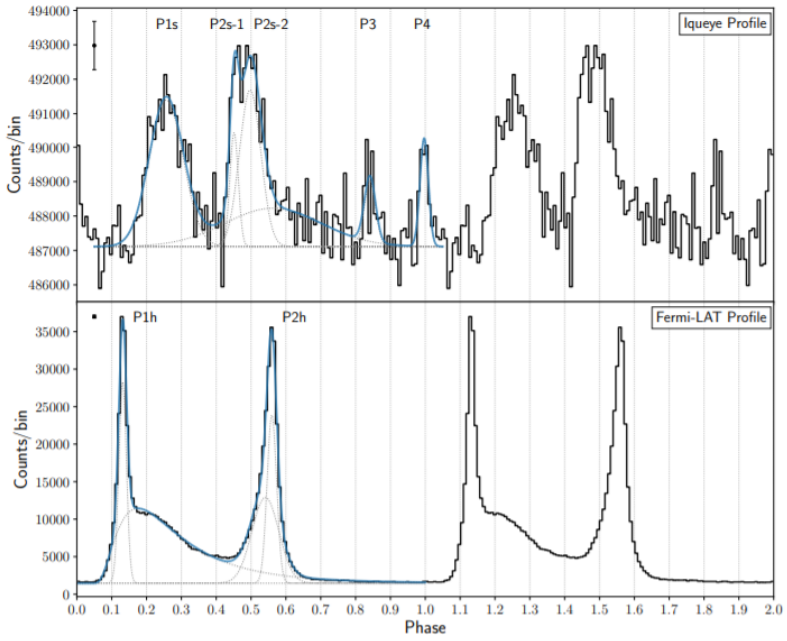

Figure 5.5: *Vela* pulse shape. The top panel correspond to the optical light curve which is shown over two cycles for clarity. The blue line shows two Gaussian functions that fit the main optical peaks [Spolon et al., 2019].

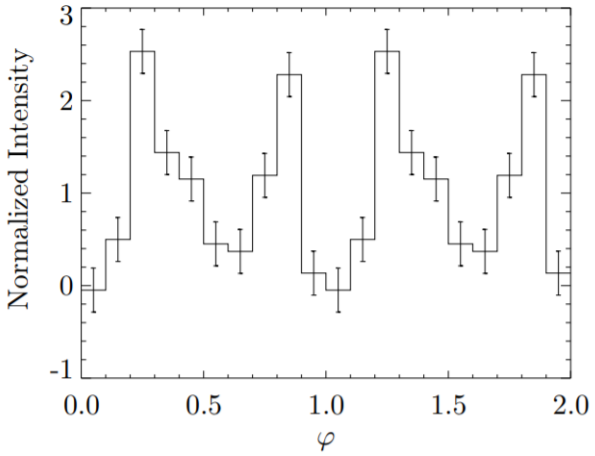

Figure 5.6: PSR $B0656+14$: pulse shape. The light curve is shown over two cycles for clarity. The error bars are 1σ errors [Kern et al., 2003].

In this respect, the best optical candidate is the *Crab* pulsar. The Crab pulsar is the brightest in this band ($V = 16.6$ mag) and it has been studied in detail. By using the phase measurement method the accuracy of the phase of the main peak will influence the accuracy of the position determination. Later in the document, the details of the accuracy analyses will demonstrate this fact. It is necessary to understand what the long term stability and the sub-μs structure of the pulse shape are in order to perform accurate optical timing of the main peak. To perform accurate optical timing it is necessary to perform a phase analysis like the one performed by Zampieri et al. [2014] or Čadež et al. [2016]. In the following section a preliminary

study of the position measurement error for the Crab pulsar is reported. Another possible candidate optical pulsar for a navigation system is PSR $B0540-69$, which is the second brightest pulsar ($V = 22.0$ mag)after the Crab pulsar.

5.3 Range measurement error for the Crab Pulsar

In the previous section the Crab nebula pulsar has been proposed as the best candidate among all the optical pulsars. In this section a preliminary estimation of the achievable accuracy of the phase measurement method using the Crab pulsar is reported. Phase measurement using one pulsar permits to estimate the error in the position of the spacecraft along the line of sight of the pulsar.

As a preliminary study on the Crab pulsar, the range measurement as a function of the observation time has been calculated and the result is reported in Figure 5.7. Different telescope diameters and a SPAD detector as instrument have been considered for the analysis. This analysis is similar to the one carried out by Sheikh et al. [2006] but adapted to our case. The equations needed to make this calculation and the values for the Crab pulsar were taken from Leeb et al. [2015].
In Sheikh et al. [2006] the range measurement error in meters is given by:

$$\sigma_{range} = c\sigma_{TOA} \tag{5.1}$$

where c is the vacuum speed of light. The σ_{TOA} is defined as:

$$\sigma_{TOA} = \frac{HWHM}{SNR} \tag{5.2}$$

where the $HWHM$ is the Half Width at Half Maximum of the main peak of the pulse shape of the Crab pulsar. The $HWHM$ value is 0.85×10^{-3} and it was taken from [Germanà et al., 2012]. The SNR is the Signal to Noise Ratio and it can be defined as:

$$SNR = \frac{N_p n_p}{\sqrt{(N_{NB} + N_D) n_p T + N_p n_p}} \tag{5.3}$$

where T is the period of the pulsar ($0.0337s$) and n_p is the number of observation periods. For N_D, which is the dark count rate, we considered 10 dark counts per second considering a cold SPAD detector. N_p is the number of photons from the source and N_{NB} is the number of photons of the nebular background. This last two values are estimated using the following equation:

$$N = tr \frac{D^2 \pi T}{4h} \int_{\nu_1}^{\nu_2} \frac{F_\nu \eta_\nu}{\nu} d\nu \tag{5.4}$$

where h is the Planck's constant, ν is the observation frequency, η_ν is the quantum efficiency, D is the diameter of the telescope and T is the pulsar period. The value tr is different for the measurement of N_{NB} (0.45) and of N_p (0.9) [Leeb et al., 2015]. F_ν is the flux of the Crab pulsar. F_ν and η_ν are taken from [Leeb et al., 2015]. They considered a SPAD detector with lower and upper frequency limits corresponding to

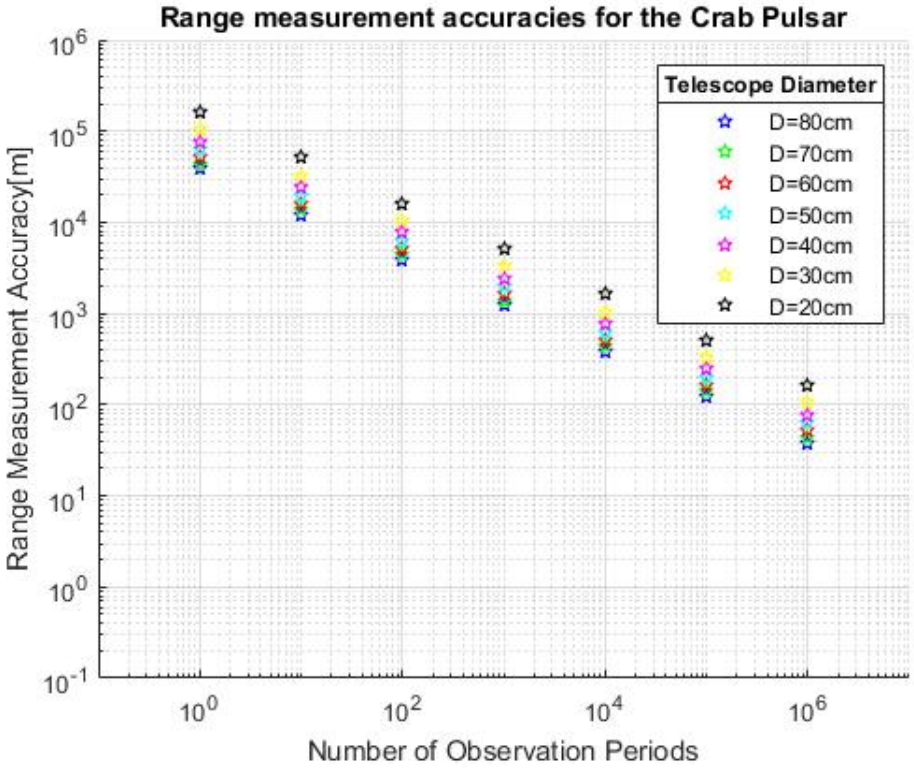

Figure 5.7: Range measurement accuracy for the Crab pulsar vs the number of observation periods considering different telescope diameters.

$\lambda = 1050nm$ and $\lambda = 400nm$ respectively. A navigation system pulsar aided should be equipped with a small telescope. In our analysis we considered different diameters of the telescope to determine how the accuracy changes. The smaller the telescope the smaller the number of acquired photons will be and therefore the longer the observation time. The result of our analysis is an accuracy of the order of 10^2 m after 10^6 observation periods, which means an observation time of the order of 10 hours.

5.4 Distribution of Pulsars

The distribution of optical pulsars in Galactic coordinates is shown in Figure 5.8. By using the phase measurement technique, the distribution of the pulsars with respect to the spacecraft is important in the process of position determination. As described in Chapter 4, the distribution of pulsars affects the accuracy of the position determination. The technique permits to determine the adjustment of the position along the line of sight of the pulsar. By using the phase measurements technique then, it is mandatory to observe at least three pulsars for a three dimensional position determination. If the navigation beacons are orthogonal each beacon is contributing maximally to the two dimensions, while if the beacons are close together the contribution to different dimensions relative to the observer is less significant. The estimate of how well distributed the pulsars are is the GDOP (Geometric Dilution of Precision).

Figure 5.8 shows the distribution of optical pulsars in the Galactic coordinate reference system. The galactic coordinate frame is the system in which the fundamental plane is the galactic plane and the origin of longitude is toward the galactic center. The pulsars reported in Figure 5.8 are the optical pulsars in Table 5.1.
It is clear that pulsars are mostly distributed along the Galactic plane. Further-

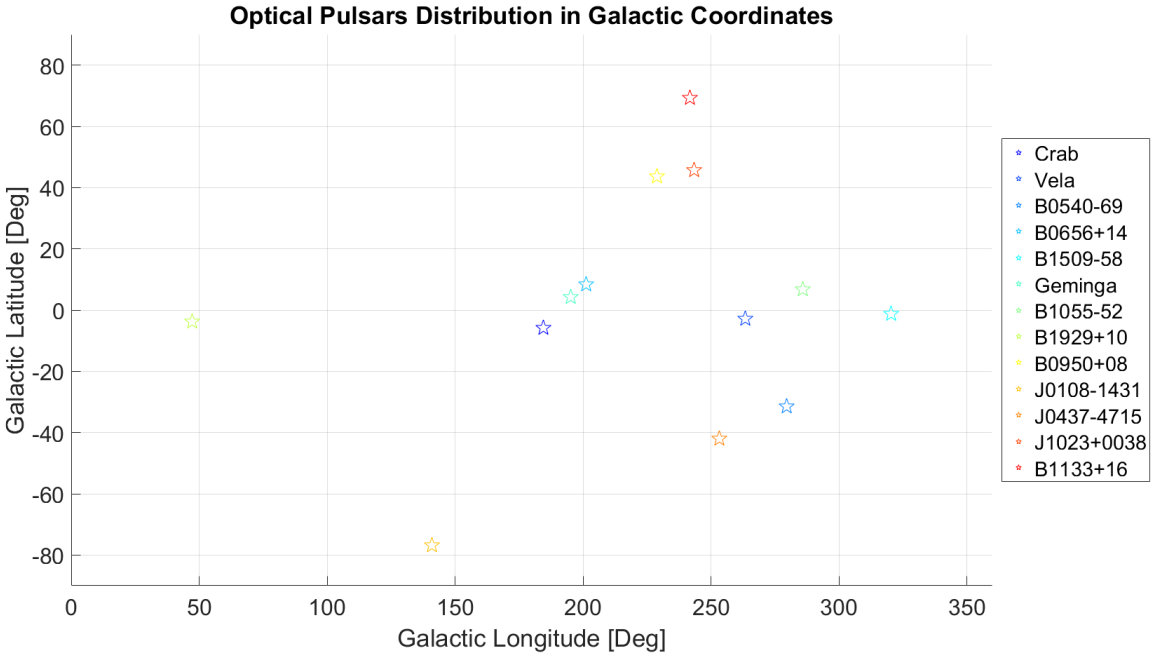

Figure 5.8: Distribution of optical pulsars in the galactic coordinates.

more, almost all pulsars are at Galactic distances. In fact, the known optical pulsars are in our Galaxy a part from PSR $B0540-69$, which is in the Large Magellanic Cloud, the closest dwarf galaxy to the Milky Way. Determination of the achievable accuracy of the phase measurement method will depend on the fact that almost all the known pulsars are along the Galactic plane.

5.5 Visibility Analysis

In this section a visibility analysis of the first six pulsars reported in Table 5.1 (those with detected pulsations) is reported. The analysis of visibility of the pulsars makes it possible to establish which sources can be observed from a satellite. In order to implement the phase measurement method it is necessary to observe at least three pulsars but, if the a-priori position of the spacecraft is unknown, at least four pulsars need to be observed in order to solve the ambiguity problem. Given the low number of optical pulsars, the question we asked was whether it is really possible to observe at least three of these simultaneously. In order to answer this question a visibility analysis has been performed.

The visibility analysis carried out is for a satellite in a circular lunar orbit (see

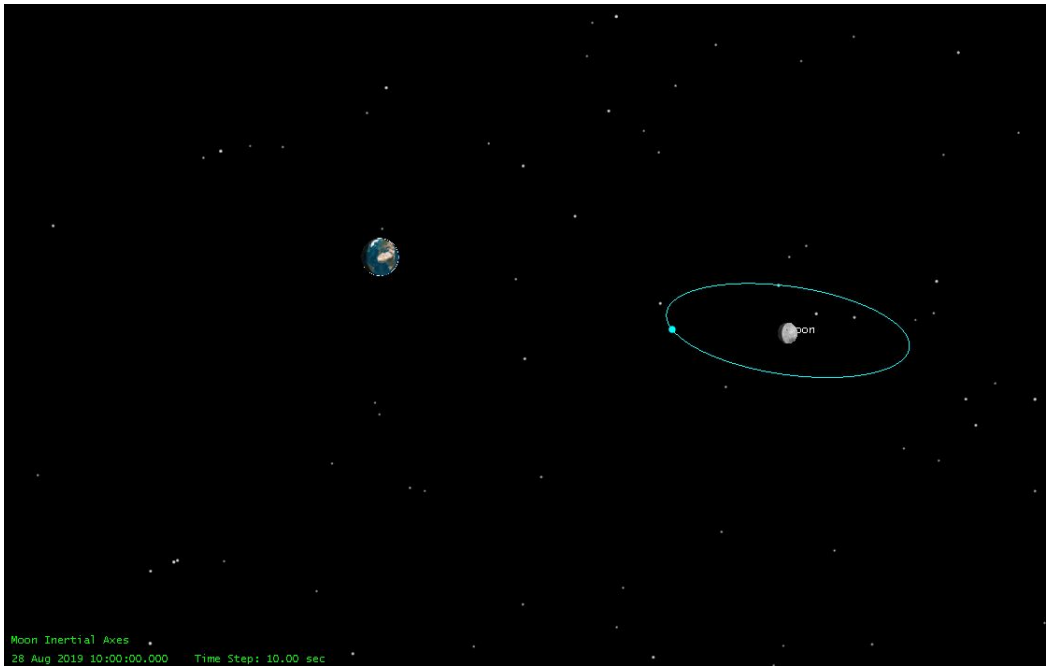

Figure 5.9: Image of a satellite in a Moon circular orbit (from STK software).

Figure 5.9).

The software that has been used is *Satellite Tool Kit* (*STK*). STK is a physics based software package from *Analytical Graphics, Inc.* that allows to perform complex analyses of ground, sea, air and space platforms. STK is a modular software which allows to use specific functions. The tool used in this case is the *access analysis*. This allows us to calculate the pulsars access from the satellite considering all the solar system objects which could stand in the line of sight from the satellite to the pulsars. Input data are the pulsars coordinates, the type of satellite orbit and the time duration during which the analysis is performed. The ephemeris of the solar system objects are already implemented in the software.
We chose a satellite in a Moon circular orbit of radius 4000 km from the Moon center. The optical pulsars selected for the analysis are (Table 5.1): *Crab*, *Vela*, *Geminga*, PSR $B0540-69$, PSR $B0656+14$ and PSR $J1023+0038$. No observable magnitude limits have been implemented. The coordinates are taken from the *ATNF catalogue* in *J2000*[3]. The time duration of the visibility analysis is one year (from 11 September 2019 to 12 September 2020).
Table 5.2 and Figures 5.10 and 5.11 show the percentage of visibility of each pulsar averaged over one year.
It is interesting to note that an occultation is possible for a satellite in a nearby lunar orbit. In particular, a periodic occultation of pulsar PSR $J1023-0038$ is produced by the presence of the Moon along the light of sight.

[3]J2000 reference frame is defined by the mean Earth's equator and equinox of the J2000 epoch.

	Visiblity Analysis
	Percentage of visibility over a year
Vela	100 %
J1023-0038	95%
Geminga	100%
Crab	100%
B0656-14	100%
B0540-69	100%

Table 5.2: Visibility analysis results. The percentage of visibility of each single optical pulsar over a year is reported.

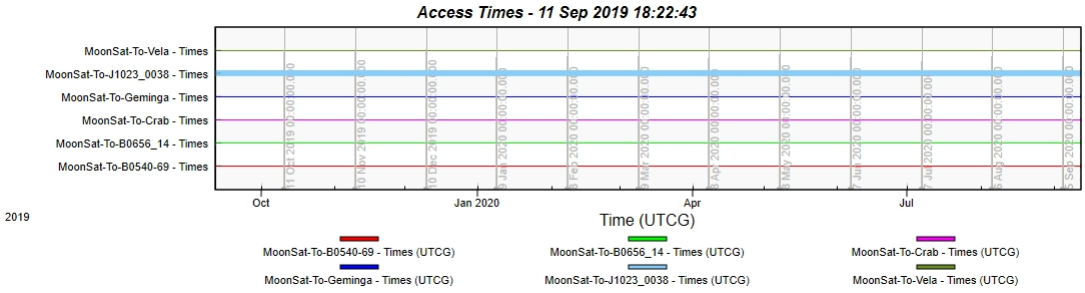

Figure 5.10: Visibility analysis results for six optical pulsars over one year (from 11 September 2019 to 12 September 2020).

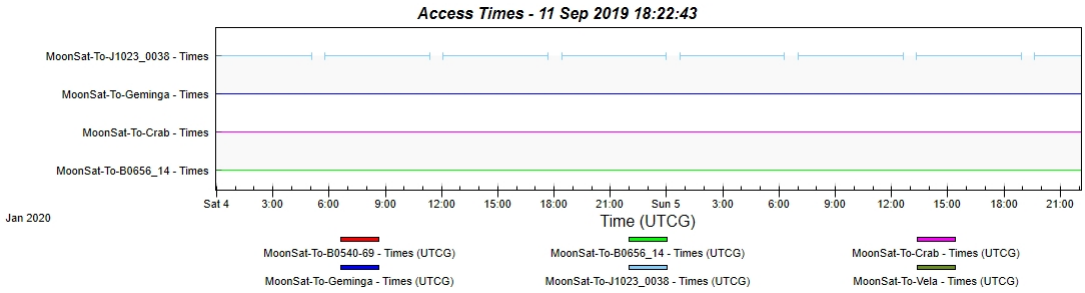

Figure 5.11: Zoom in of image 5.10. It shows that the pulsar PSR $J1023-0038$ is periodically occulted by the Moon.

6. Results: Theory

In this chapter the accuracy analyses that have been carried out in order to determine the achievable accuracy of a pulsar navigation system are reported. The accuracy analyses for the determination of positions and velocity with the ToA (Time of Arrival) method and the Drift-ToA method, respectively, of the spacecraft have been performed by using two mathematical techniques: *weighted least squares* and *extended Kalman filter*. The first allows to investigate the accuracy of the ToA method in an Epoch-by-Epoch approach, which means that the estimate of the accuracy in the position determination is made considering a single observation at a defined epoch. The second allows to investigate the accuracy in an iterative approach, thus the navigation solution is continuously searched during the motion of the spacecraft by continuously observing the pulsars. This chapter is divided in two main sections. In the first section the mathematical theories necessary to understand the results are reported. In the second part the description of the performed accuracy analyses and the discussion of the results are reported.

6.1 Mathematical Theory

The first step of our analysis was the estimate of the achievable accuracy of a pulsar navigation system in the spacecraft position and velocity determination process. In particular the aim of the thesis is the determination of the achievable accuracy using optical pulsars. To reach the proposed aim we acted in two directions: accuracy analyses and measurements using real data (see Chapter 7). In this chapter the first investigation that has been pursued is reported: accuracy analyses considering the errors involved in the ToA measurement and Drift-ToA for position, velocity and clock error determination. This analysis does not need real ToA and Drift-ToA measurements. The demonstration of this fact is reported in the following two subsections. For our purpose, the interest is in the derivation of the covariance matrices and not in the determination of the unknown parameters vector. Equations reported in Chapter 4 are useful to understand what are the parameters that influence the measurements for the determination of the unknown quantities. The theory here explained is not complete, it focuses on the points of our interest and it is partly taken from Subirana et al. [2013] and Teunissen et al. [2008].

6.1.1 Weighted Least Square

Weighted least squares (WLS), or weighted linear regression, is a generalization of ordinary least squares. WLS is an estimation method that permits to obtain the unknown parameter vector $\mathbf{x}$. A system of linear equations can be written for simplicity as follow:

$$\mathbf{y} = \mathbf{G}\mathbf{x} + \mathbf{w_y} \tag{6.1}$$

where $\mathbf{y}$ is the measurement vector, $\mathbf{G}$ is the geometry matrix of the system, $\mathbf{x}$ is the unknown parameter vector and $\mathbf{w_y}$ is the measurement error term. Because of the error term, equation (6.1) has no exact solution fulfilling the system. To find the best estimate, $\hat{x}$, of $\mathbf{x}$, where $\hat{\mathbf{x}}$ is the vector that minimises the discrepancy in the equations system, we can write the equation:

$$\widehat{\mathbf{y}} = \mathbf{G}\widehat{\mathbf{x}}. \tag{6.2}$$

The least squares estimation method is defined by the following condition:

$$min\|\mathbf{y} - \widehat{\mathbf{y}}\|^2 = min[\sum_{i=1}^{n}(y_i - \widehat{y_i})^2]. \tag{6.3}$$

Thus, the least squares estimator solution defined by equation (6.3) gives the vector $\widehat{\mathbf{y}}$ that minimises the residual quadratic norm $\|\mathbf{r}\|^2 = \|\mathbf{y} - \widehat{\mathbf{y}}\|^2 = \|\mathbf{y} - \mathbf{G}\widehat{\mathbf{x}}\|^2$, where $\mathbf{r}$ is the post-fit residual. From linear algebra the solution that fulfils the condition (6.3) is given by:

$$\widehat{\mathbf{x}} = (\mathbf{G^T G})^{-1}\mathbf{G^T y} \tag{6.4}$$

where the exponent $\mathbf{T}$ stands for transposed matrix.
By substituting equations (6.4) and (6.1) in $\mathbf{r}$, the post-fit residual becomes:

$$\mathbf{r} = [\mathbf{I} - \mathbf{G}(\mathbf{G^T G})^{-1}\mathbf{G^T}]\mathbf{y} = \mathbf{S}\mathbf{y} \tag{6.5}$$

where $\mathbf{I}$ is the identity matrix and $\mathbf{S}$ is a symmetric and idempotent matrix:

$$\mathbf{S} = \mathbf{I} - \mathbf{G}(\mathbf{G^T G})^{-1}\mathbf{G^T}, \mathbf{S^T} = \mathbf{S}, \mathbf{S^2} = \mathbf{S}. \tag{6.6}$$

If we assume that the pre-fit residuals have mean zero errors $E[\mathbf{w_y}] = 0$ and having defined their covariance matrix as $\mathbf{R}$, then the mean error $\mathbf{m}$ and the covariance matrix $\mathbf{P}$ of the estimate are given by:

$$\begin{aligned}
\mathbf{m} &= E[\widehat{\mathbf{x}} - \mathbf{x}] = (\mathbf{G^T G})^{-1}\mathbf{G^T}E[w] = 0 \\
\mathbf{P} &= E[(\widehat{\mathbf{x}}-\mathbf{x})(\widehat{\mathbf{x}}-\mathbf{x})^T] = (\mathbf{G^T G})^{-1}\mathbf{G^T G}E[\mathbf{w_y w_y^T}](\mathbf{G^T G})^{-1} = (\mathbf{G^T G})^{-1}\mathbf{G^T R G}(\mathbf{G^T G})^{-1} \\
MSE &= E[(\widehat{\mathbf{x}} - \mathbf{x})^T(\widehat{\mathbf{x}} - \mathbf{x})] = tr(\mathbf{P}).
\end{aligned} \tag{6.7}$$

In the assumption of uncorrelated values with identical variance σ^2 hence $\mathbf{R} = E[\mathbf{w_y w_y^T}] = \sigma^2\mathbf{I}$, then the last two equations in (6.7) become:

$$\mathbf{P} = \sigma^2(\mathbf{G^T G})^{-1}, MSE = \sigma^2 tr[(\mathbf{G^T G})^{-1}]. \tag{6.8}$$

In this work all measurements have been treated in the same way. In a real scenario not all the measurements have the same error. It is possible to introduce a weighting matrix $\mathbf{W}$, which is symmetric and positive definite, and redefine the least squares conditions as:

$$min\|\mathbf{y} - \widehat{\mathbf{y}}\|_W^2 \tag{6.9}$$

where the norm of the residual vector is associated with scalar product defined by the weighting matrix.
The estimator and its covariance matrix now become:

$$\widehat{\mathbf{x}}_W = (\mathbf{G^T W G})^{-1}\mathbf{G^T W y} \tag{6.10}$$

$$\mathbf{P}_W = (\mathbf{G^T W G})^{-1}\mathbf{G^T W R W G}(\mathbf{G^T W G})^{-1} \tag{6.11}$$

It is important to notice that the covariance matrix in both cases does not depend on the measurement vector $\mathbf{y}$. This fact implies the possibility to perform covariance analyses without the need of real data or simulated measurements. The aim is to make an a-priori covariance analysis of the problem in order to define the achievable accuracy and determine which are the more important contributions to the measurements error.
It is possible to simplify the last two equations taking the weighting matrix $\mathbf{W}$ as the inverse of the covariance matrix $\mathbf{R}$:

$$\mathbf{W} = \mathbf{R}^{-1}. \tag{6.12}$$

If we substitute (6.12) in equations (6.10) and (6.11) our final equations become:

$$\widehat{\mathbf{x}} = (\mathbf{G^T R^{-1} G})^{-1}\mathbf{G^T R^{-1} y} \tag{6.13}$$

$$\mathbf{P} = (\mathbf{G^T R^{-1} G})^{-1}. \tag{6.14}$$

This solution corresponds to the Best Linear Unbiased Minimum Variance Estimator (BLUE) [Subirana et al., 2013]. It is possible, if the measurements are uncorrelated, to define the weighting matrix $\mathbf{W}$ as follow:

$$\mathbf{W} = \begin{bmatrix} 1/\sigma_{y_1}^2 & 0 & 0 \\ 0 & \ddots & 0 \\ 0 & 0 & 1/\sigma_{y_n}^2 \end{bmatrix} \tag{6.15}$$

where $\sigma_{y_i}^2$ are the sum of uncertainties of the different error sources (clock, timing noise, etc.) and i stands for the i-th pulsar.

6.1.2 Extended Kalman Filter

The *Extended Kalman Filter*(EKF) is the non-linear version of the *Kalman filter* (KF) which linearizes the system equations. After the linearization, the EKF equations are identical to the KF ones. The linear equations of the system have already been derived in Chapter 4. *Kalman Filter* is an estimation method, routinely used

in navigation systems. The name of this estimation theory comes from the primary developer of the theory Rudolf E. Kalman.
The principle of the *Kalman filter* (KF) can be roughly described as the WLS solution of the linearised observation system augmented with a prediction of the estimate as additional equations. KF is an algorithm that uses a series of measurements observed over time and produces estimates of unknown variables that are more accurate than those based on a single measurement. The algorithm works in a two step process: *prediction* and *update*. In the prediction step, the estimates of the current state variables and their uncertainties are produced. Once the next measurement is observed the estimates are updated using a weighted average. The algorithm is recursive. KF needs a system's dynamic model which means that it needs as input physical laws of motion and multiple sequential measurements to form an estimate of the system's varying quantities. This estimate would be better than the estimate obtained by using a single measurement. KF produces the estimate of the state of the system as an average of the system's predicted state and the new measurement using a weighted average. The weights are calculated from the covariance, which is the measure of the estimated uncertainty of the prediction of the system's state. The results of the weighted average are a new state estimate that is between the predicted and measured state. This process is repeated recursively, updating at each iteration the new estimate and its covariance for the following iteration. KF does not need the entire history to calculate the new state but only the last best estimate state. An important term is the Kalman filter's gain. The Kalman gain is the relative weight given to the measurements and the current state estimate. With a high gain the filter places more weight on the most recent measurements and with a low gain the filter follows the model predictions more closely. In the actual implementation of the filter, the state estimate and covariances are matrices. These matrices represent a linear relationship between the state variables and the measurements. If the relationship is not linear then the extended Kalman filter (EKF) needs to be used. In order to use the Kalman filter the following matrices need to be defined:

- A_k is the state transition model matrix where the physical laws of the system are;
- G_k is the observation model matrix (or geometry matrix);
- Q_k is the covariance matrix of the process noise;
- R_k is the covariance matrix of the observation noise;

The Kalman filter assumes that the true state x_k is evolved from the previous state x_k^- according to:

$$x_k = A_k x_k^- + w_k \tag{6.16}$$

where A_k is the state transition model applied to the previous state x_k^- and w_k is the process noise which can be assumed to be zero mean Gaussian with covariance Q_k ($w_k \sim N(0, Q_k)$).
The measurement y_k of the true state x_k is made according to:

$$y_k = G_k x_k + v_k \tag{6.17}$$

where G_k is the geometry matrix that relates the measurements and the unknown parameters, and v_k is the observation noise which can be assumed to be zero mean Gaussian with covariance R_k ($v_k \sim N(0, R_k)$). As explained above, the KF works in two steps. The first step is the *prediction measurement*:

$$\hat{x}_k^- = A_k \hat{x}_{k-1}; \tag{6.18}$$

$$P_k^- = A_k P_{k-1} A_k^T + W_k Q_{k-1} W_k^T \tag{6.19}$$

where $\hat{x}_k^-$ is the predicted state estimate and P_k^- is the predicted error covariance with W_k a weighting matrix.
The second step is called *update* and the equations are the following. The measurement pre-fit residual $\tilde{y_k}$ and its covariance, S_k, are:

$$\tilde{y_k} = y_k - G_k \hat{x}_k^-;$$

$$S_k = G_k P_k^- G_k^T + R_k. \tag{6.20}$$

The optimal Kalman gain is given by:

$$K_k = P_k^- G_k^T S_k^{-1}; \tag{6.21}$$

Only after determination of the above matrices is it possible to determine the updated state estimate $\hat{x}_k$, its covariance, P_k, and the post-fit residual measurements, $\tilde{y_k}$:

$$\hat{x}_k = \hat{x}_k^- + K_k \tilde{y_k};$$

$$P_k = (\mathbf{1} - K_k G_k) P_k^-;$$

$$\tilde{y_k} = z_k - G_k \hat{x}_k. \tag{6.22}$$

As already said above, the Kalman gain can be chosen depending on the system. Here, the updated estimate covariance is valid for the optimal Kalman gain that minimizes the residual error.

6.2 Results of the WLS

In this section the results of the accuracy analysis done using the WLS theory are reported. The theory equations are reported in Section 6.1.1. The method considered is the phase measurement described in Section 4, where the equations of the system are reported. The method permits to determine the achievable accuracy of phase measurement in three dimension and the clock error.

Determination of the achievable accuracy is done by determining the covariance matrix of the system, called $\mathbf{P}$. The computing environment utilized to compute the covariance matrices is $MATLAB$[1], a language developed by MathWorks. As already

[1] https://www.mathworks.com/products/matlab.html

demonstrated in Section 6.1.1, it is possible to determine the covariance matrix of the system without simulation of the measurements. The input needed in the computation is first of all the geometry matrix of the system. The geometry matrix of the problem is (4.14) which depends on the coordinates of the selected pulsars:

$$\mathbf{G} = \begin{bmatrix} -\frac{\widehat{u}_1^x}{c} & -\frac{\widehat{u}_1^y}{c} & -\frac{\widehat{u}_1^z}{c} & 1 \\ \vdots & & & \vdots \\ -\frac{\widehat{u}_k^x}{c} & -\frac{\widehat{u}_k^y}{c} & -\frac{\widehat{u}_k^z}{c} & 1 \end{bmatrix}; \tag{6.23}$$

here k stands for the k-th pulsar, the first three columns are associated with the spatial variables, while the last column is associated with the time variable.
$\widehat{u}_n^x$, $\widehat{u}_n^y$, $\widehat{u}_n^z$ are the unit vector components of each pulsar from the pulsar to the SSB. Their values are calculated by using trigonometric equations and the input coordinates are the right ascension (α) and the declination (δ) in $J2000$ reference frame taken from *ATFNcatalogue*. Another input matrix required by the theory is the initial covariance matrix of the measurement, previously called $\mathbf{R_y}$. The covariance matrix, equation (4.19), is a diagonal matrix whose values correspond to the sum of all the contributing errors in the measurement. There are two main assumptions in this analysis. We assumed the possibility of observing more than one pulsar at a time and we did not consider the unknown integer number of pulses in the detection as one of the unknown parameters in the unknown parameter vector, hence the ambiguity problem is assumed to be solved. The contributing errors to the measurements and the values considered in the analysis are the following:

- σ_{ToA}: it is the error in the determination of the phase of the pulse profile peak. In this case we adopted the value given by Germanà et al. [2012]. The value, $\sim 30\mu$s corresponding to $\sim 1/1000$ of the period, is the small 1-σ uncertainty on the position of the main peak of the Crab nebula pulsar determined using the Aqueye instrument mounted on the Copernicus telescope in Asiago. We used the same value for all the pulsars even if it is a strong assumption.

- σ_{SSB}: it is the error in the determination of the pulse shape template at the SSB. The Jodrell Bank observatory gives the monthly ephemeris in the radio band only of the Crab pulsar. The RMS (root mean square) timing residual used in this analysis is 1.2×10^{-3} in milliperiods. The value is an average on the RMS given by Jodrell Bank observatory for the Crab pulsar. We used the same value for all the pulsars multiplying it for the different pulsar periods, even if it is a strong assumption.

- σ_{OR}: it is the error made in the comparison between the optical measurements and the radio template. As already explained, a delay has been found between radio and optical ToA measurements of the Crab pulsar. At the spacecraft measurements are taken with an optical telescope while the ephemeris needed for the reconstruction of the template at the epoch of observation are in the radio band. The value, 6.0μs, is given by Germanà et al. [2012] for the Crab nebula pulsar. We chose to adopt this value for all the pulsars even if it is a strong assumption.

- σ_{DM}: it is the error in the determination of the delay due to the interstellar medium. As already explained, this delay affects only the radio photons. Even though the measurements at the spacecraft are made in the optical band the ephemeris needed for the template are in the radio band. The value, 5.0×10^{-2} $\mathrm{cm}^{-3}\mathrm{pc}$, is taken from the ATNF pulsar database and it is valid for the Crab pulsar. We used the same value for all the pulsars.

- σ_{clock}: it is the uncertainty due to the spacecraft clock drift. If the spacecraft clock deviates, the measurement of the ToA will be affected. The chosen value is 1.0×10^{-9} s.

The equation implemented in the program for the determination of the covariance matrix of the system is the following:

$$\mathbf{P} = (\mathbf{G^T R^{-1} G})^{-1}$$

where $\mathbf{G}$ is the geometry matrix, previously defined, and $\mathbf{R}$ is a diagonal matrix whose values are the sum of the square of the uncertainties defined above.
The performed analysis considers different pulsar sets:

- Pulsar Set **1**: *PSR B0531+21 (Crab)*, *PSR B0833-45 (Vela)*, *PSR B0540-69*, *PSR B0656+14*;

- Pulsar Set **2**:*PSR B0540-69*, *PSR B0656+14*, *PSR B1509-58*, *PSR J0633+1746 (Geminga)*;

- Pulsar Set **3**: *PSR B0531+21 (Crab)*, *PSR B0833-45 (Vela)*, *PSR B0540-69*, *PSR B0656+14*, *PSR B1509-58*, *PSR J0633+1746 (Geminga)*;

- Pulsar Set **4**: *PSR B0531+21 (Crab)*, *PSR B0833-45 (Vela)*, *PSR B0540-69*, *PSR B0656+14*, *PSR B1509-58*, *PSR J0633+1746 (Geminga)*, *PSR B1055-52*, *PSR B1929+10*, *PSR B0950+08*, *PSR J0108-1431*, *PSR J0437-4715*, *PSR J1023+0038*, *PSR B1133+16*.

The results of the analysis are reported in Table 6.1. Performing the analysis considering several pulsar sets gives the possibility to study the variation of the GDOP (Geometry dilution of precision). The GDOP is a measure of how well the sets of pulsars are chosen. The accuracy of the time variable is called TDOP, Time Dilution of Precision, while the accuracy for the three dimension position determination is called PDOP, Position Dilution of Precision. In this analysis different pulsar sets have been considered in order to verify that the accuracy of the position determination depends also on the distribution of the pulsars. The GDOP is calculated from the covariance matrix, in detail it is the square-root of the sum of the values in the diagonal of the covariance matrix. The TDOP value is the square-root of the last value on the diagonal of the estimated covariance matrix divided by c, the vacuum speed of light, in order to have the value in unit of s. The PDOP value is the square-root of the sum of the three position value of the estimated covariance matrix.
The GDOP column in Table 6.1 shows the fact that a different set of pulsars can lead to different accuracies. For example, pulsars sets number 1 and 2 consider the

Accuracy Analysis with WLS			
Pulsars Set	TDOP [s]	PDOP [m]	GDOP [m]
1	1.86×10^{-4}	$1.41 \times 10^{+5}$	$1.52 \times 10^{+5}$
2	3.57×10^{-4}	$5.61 \times 10^{+5}$	$5.71 \times 10^{+5}$
3	1.72×10^{-4}	$1.34 \times 10^{+5}$	$1.44 \times 10^{+5}$
4	1.29×10^{-4}	$8.38 \times 10^{+4}$	$9.24 \times 10^{+4}$

Table 6.1: Results of the accuracy analysis with WLS estimation method using different pulsar sets. The TDOP indicates the achievable accuracy of the time variable while the PDOP indicates the achievable accuracy for the three dimension position. The GDOP provides a measure on how well the different set of pulsars are chosen.

same number of pulsars, i.e. four pulsars, but different pulsars are chosen for the two different sets. The GDOP and the PDOP values are different, in particular the first one is better than the second one. This can be considered as proof that the accuracy in determining the spacecraft position is influenced by the position of the pulsars in the sky. The best result is the one calculated considering pulsar set number 4. In this set the pulsars considered are nine. By considering observation of nine pulsars means that the spacecraft is equipped with the useful instrumentation for observation of nine sources. This instrumentation will be very complex and difficult to realize. However, the result in this case gives an accuracy on the position determination of the order of 10 km. The following consideration are useful to understand this result. The dominant uncertainty for the determination of the pulsar navigation system is the pulse peak phase determination (σ_{ToA}). From the theory of the phase measurement the phase shift corresponds to a range difference Δx along the line of sight toward the observed pulsar, as explained in Chapter 4. Consequently an error in the phase peak determination leads to an error on the spacecraft position determination. It is clear that a timing residual of the order of 10μs leads to a position error of about 3 km. The WLS analysis gives proof of this fact. The σ_{ToA} considered is 30μs which leads to a position error of ten km in the best case (pulsar selection number 4). The assumed σ_{ToA} value is valid for the Crab pulsar which is the more studied among all the optical pulsars. Such large uncertainty is due to the timing noise of the pulsar. The timing noise is more important if the observation time is of several hours. We will go into the details of the timing noise in Chapter 7, where the analysis on the Crab pulsar real data is reported.
The analysis reported here is weak due to the large assumptions made in the definition of the uncertainties. We made strong assumptions because not all the data we needed for this analysis are available in the literature. It is the first time that an optical pulsars navigation system is proposed and the analyses carried out have never been performed before. For this reason it has been difficult to find the value to carry out the analysis properly. However, the analysis gives an important result which agrees with the theory. The achievable accuracy is firstly dominated by the phase peak determination uncertainty.
The results of WLS analysis show that single observations of different pulsars lead to an accuracy of kilometres at the most. The in-orbit demonstration of X-ray pulsars navigation system carried out to date and described in Chapter 3, gives as result an achievable accuracy of the spacecraft position determination of about 10 km.

The results of this analysis agree with those in the literature. However, in order to verify if it is possible to improve the accuracy another estimation technique has been implemented. In the next section the reported accuracy analysis shows that it is possible to improve the estimate position error using a different approach. The idea was to improve the results of this analysis using an iterated approach instead of a single epoch approach like the one of the WLS.

6.3 Results of the EKF

In this section the results of the accuracy analysis done using the extended Kalman filter theory are reported. The theory equations, which allow calculation of the accuracy, are reported in Section 6.1.2. The navigation method considered is phase measurement described in Section 4, where the equations of the system are reported. The method allows the determination of the achievable accuracy of phase measurement in three dimension, the accuracy in the velocity determination and the clock error. The computing environment utilized to compute the covariance matrices is *MATLAB*, a language developed by MathWorks. As already demonstrated in Section 6.1.2, it is possible to determine the covariance matrix of the system without simulation of the measurements.

As reported in Section 6.1.2, for the implementation of the Kalman filter the definition of various matrices is mandatory. The matrix A_k is the state transition model matrix. The physical law of the motion of the satellite is described in this matrix. The physical law considered in this analysis is the one of uniform straight motion:

$$A = \begin{bmatrix} \mathbf{I}_{3\times3} & T_s\mathbf{I}_{3\times3} & 0 \\ 0 & \mathbf{I}_{3\times3} & 0 \\ 0 & 0 & 1 \end{bmatrix} \tag{6.24}$$

where T_s is the sampling time i.e. the observation time and $\mathbf{I}_{3\times3}$ is the identity matrix. Matrix G_k is the observation model matrix i.e. the geometry matrix. The geometry matrix of the system has already been reported in the previous section, see equation 6.23. In this matrix there are the unit vectors from the pulsars to the SSB. Matrix R_k is the covariance matrix of the observation noise. The initial covariance matrix has already been defined in the previous section. R is a diagonal matrix whose values are the sum of the square of the uncertainties already defined in the previous section: σ_{ToA}, the uncertainty of the phase peak; σ_{SSB}, the uncertainty of the determination of the template at the SSB; σ_{OR} the uncertainty of the comparison between the radio template and the optical measure; σ_{DM}, the uncertainty of the dilution measure; and σ_{Clock}, the spacecraft clock error. Matrix Q_k is the covariance matrix of the process noise:

$$Q = \begin{bmatrix} T_sW_v\mathbf{I}_{3\times3} & 0_{3\times3} & 0 \\ 0_{3\times3} & T_sW_v\mathbf{I}_{3\times3} & 0 \\ 0 & 0 & T_sW_e \end{bmatrix} \tag{6.25}$$

where T_s is the sampling time i.e. the observation time and $\mathbf{I}_{3\times3}$ is the identity matrix. W_v is an independent zero mean white noise of the process with a known power

spectrum density related to velocity determination. W_e is an independent zero mean white noise of the process with a known power spectrum density related to time determination. W_v and W_e values are taken from Emadzadeh and Speyer [2010] and they are: $W_v = 10^{-12} m^2/s$ and $W_e = 10^{-12} s$.
EKF needs an initial covariance matrix to initialize implementation. The initial covariance matrix is taken from the result of the WLS accuracy estimation. In detail, in this method we used the results of the pulsar set number 1 of the WLS analysis. We choose pulsar set number 1 (*PSR B0531+21 (Crab)*, *PSR B0833-45 (Vela)*, *PSR B0540-69*, *PSR B0656+14*) because a system that can observe at most four pulsars is more feasible for the required instrumentation, compared for example to pulsars set number 4 which uses nine pulsars. Moreover, the result of the WLS accuracy analysis carried out with pulsar set number 1 gives a higher GDOP value compared to pulsar set number 2 in which four pulsars are used in this case as well. The results of the Kalman filter are reported in the following plots.
In our analysis we considered two different sampling times: 500 s and 10 s. These numbers, actually, are merely a supposition because the correct way to carry out this analysis would require the knowledge of the suitable dimensions of the telescope. The diameter of the telescope will influence the results. In fact, the sampling time to be chosen depends on the number of photons which are needed for the reconstruction of the pulse shape of the signal. The number of photons acquired would depend on the area of the instrument.
Figures 6.1 and 6.2 show the achievable accuracy of the position estimate using the two different sampling times. The accuracy of determination of the position are

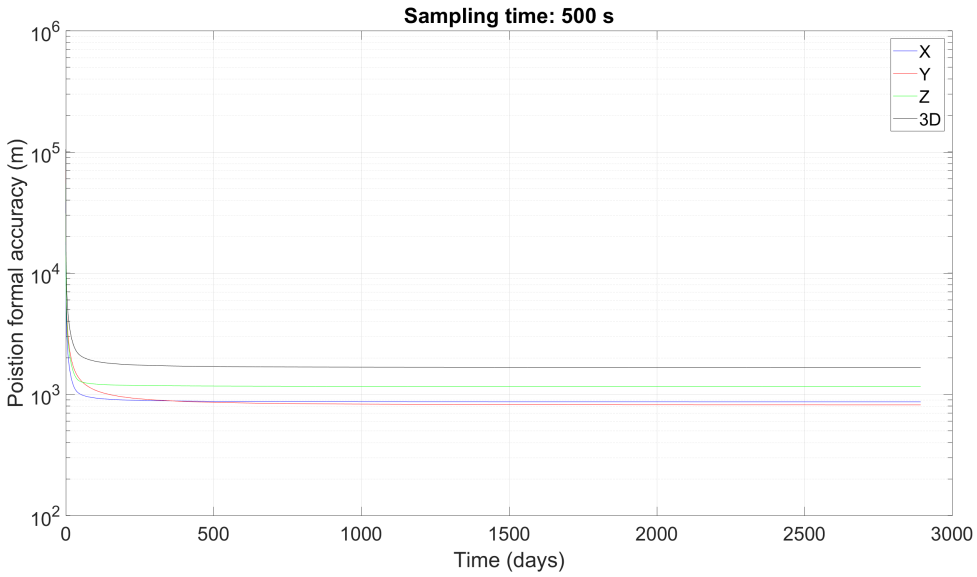

Figure 6.1: Position accuracy analysis results using EKF and 500 second of time sampling.

plotted in the figures of the position along x, y and z axis and the three dimension together. The position determination along x axis is better compared to the z and y axes in both cases. This fact could be connected with the distribution of the pulsars, already discussed in Section 5. By considering a sampling time of 10 s the result is

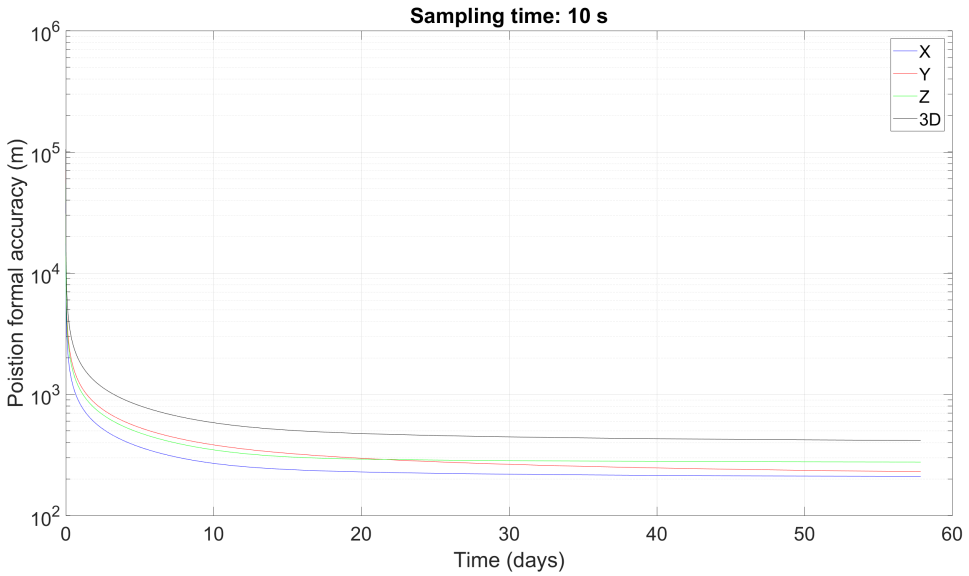

Figure 6.2: Position accuracy analysis results using EKF and 10 second of time sampling.

much better compared to the one with a sampling time of 500 s. However, a sampling time of 10 s is quite short considering that pulsars are faint objects, consequently 10 s is a strong assumption. The achievable accuracy of the phase measurement method is $\sim 5 \times 10^2$ m after 20 days of iterated observation with a sampling time of 10 s. This results is definitely better than that achieved with the WLS method, which used a single epoch approach.

Figures 6.3 and 6.3 show the achievable accuracy of the velocity estimate using the two different sampling times. The accuracy of determination of the velocity

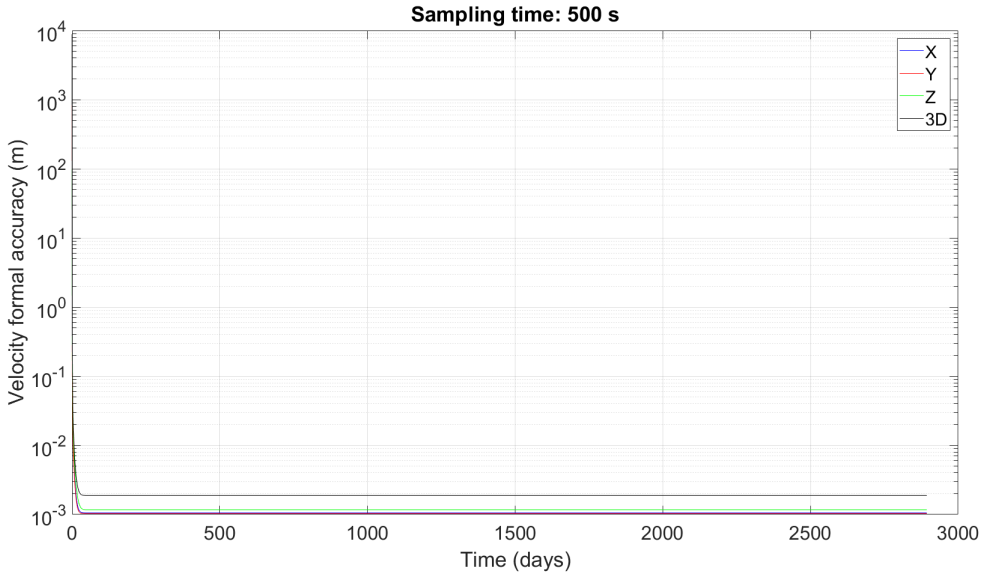

Figure 6.3: Velocity accuracy analysis results using EKF and 500 second of time sampling.

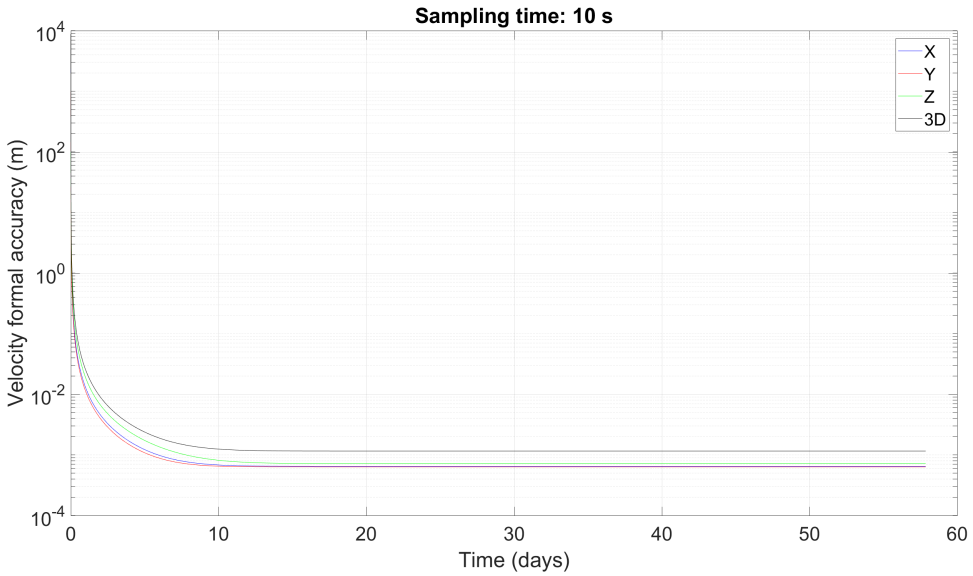

Figure 6.4: Velocity accuracy analysis results using EKF and 10 second of time sampling.

components are plotted in the figures along the axis x, y, z and the three dimension together. In this case the sampling time of 500 s and 10 s does not influence in an important way as in the case of the determination of the position. The achievable accuracy of the velocity determination is $\sim 10^{-3}$ m/s after 20 days in the case of the sampling time equals to 10 s.

Figures 6.6 and 6.5 show the achievable accuracy of the time estimate using the two different sampling times. Even in this case, like in the case of the velocity esti-

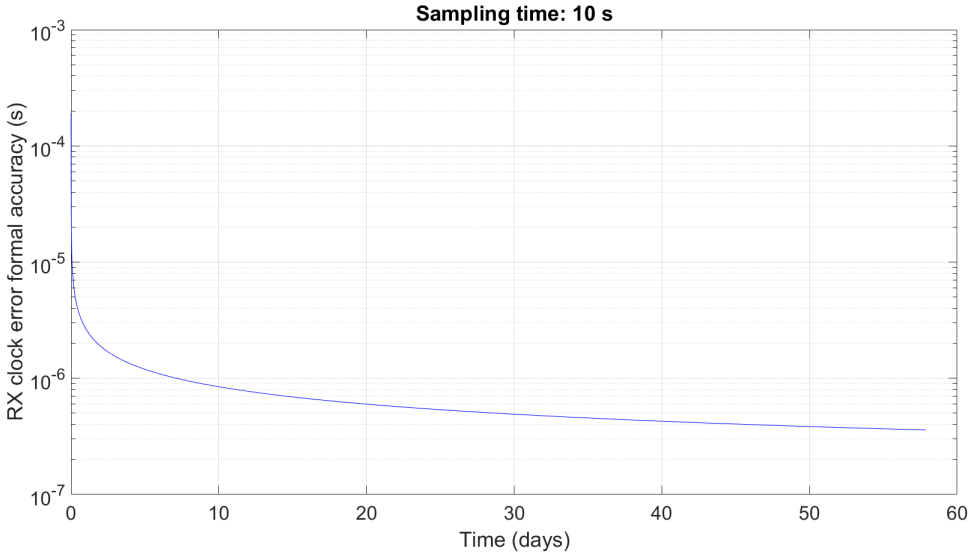

Figure 6.5: Time accuracy analysis results using EKF and 10 second of time sampling.

mate, the chosen sampling time does not seem to influence the accuracy to a great extent as in the case of the position accuracy. The achievable accuracy of the clock

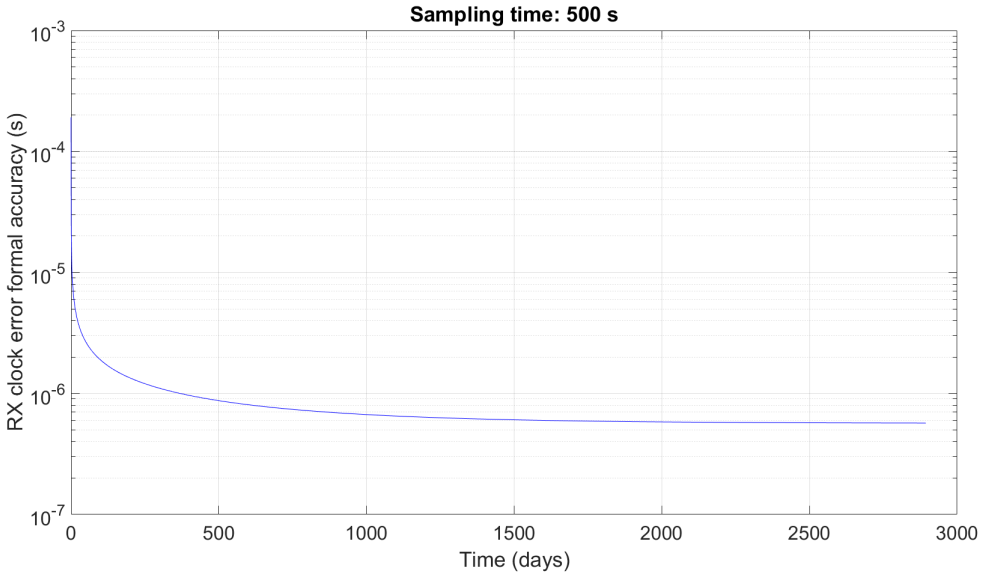

Figure 6.6: Time accuracy analysis results using EKF and 500 second of time sampling.

error estimate is $\sim 10^{-6}$ s after 20 days of observation.

The purpose of the EKF analysis was to verify that an iterated approach in the position determination of the pulsars navigation system was better compared to an epoch-by-epoch approach. It is possible to conclude that the results of the extended Kalman filter analysis are better than the results of the WLS analysis. By comparing the results of the WLS analysis in the case of pulsars set number 1 and the results of the EKF this conclusion is easily verifiable. The EKF analysis is similar to the one carried out by Thameemunnisha and Ramachandran [2016] in which they considered X-ray pulsars. The results of their analysis are similar to the ones reported in this analysis. In detail, we can conclude that the iterated approach gives better results of the epoch-by-epoch approach. An iterated approach is feasible considering any type of mission. In any case, the results of the two analyses give the same important result: the uncertainty of the determination of the phase of the pulse shape peak defines the accuracy limits of the method of the phase measurements. A further study on the analysis here reported would be required in order to understand which is the ideal sampling time for an optical pulsars navigation system. In order to understand if it is possible to reach better accuracy on the spacecraft position determination an analysis on real data has been carried out. Moreover, this analysis gives a better explanation over the timing noise problem. In the next chapter an analysis on real data of the Crab pulsar is reported. In this analysis both the phase measurement and SEPO methods will be considered.

7. Results: Measurements on the Crab pulsar

In this chapter the results of the carried out analyses are reported considering real data of the Crab nebula pulsar. The aim of this analysis is assessing the feasibility of a pulsar navigation system considering the optical pulsations of the Crab pulsar. In particular, the analysis deals with the ToA and the SEPO methods, reported in Sections 7.2 and 7.3, respectively. The optical data were obtained using the 1.82 m Copernicus telescope at the Asiago observatory. The description of the data reduction and the data analysis are reported in Section 7.1.

7.1 Data Reduction

The reported analysis has been performed with real data of the Crab pulsar. Only twelve of all the known pulsars (~ 2000) show optical emission at detectable levels and among them only six show pulsations in the optical band. The choice of the pulsar to analyse is made on the basis of the arguments reported in Chapter 5. In the case of the visual band the best candidate for an optical pulsar navigation system is the Crab nebula pulsar. Although this is not a millisecond pulsar, in fact it shows a higher period derivative ($dP/dt \sim 4.21 \cdot 10^{-13}$ s/s) compared to the millisecond typical one, it is the brightest pulsar in the visual band ($V \sim 16.6$ mag). Moreover, it is the most studied among all the pulsars in the different wavelengths. Its optical light curve is characterized by a double peak profile and it is very stable. It has been found that the pulse shape is stable at the level of $\sim 1\%$ on a timescale of 14 years [Zampieri et al., 2011]. Nevertheless, the pulsar spin-down has a complex behaviour: significant phase noises as glitches, jumps and random walks in frequency have been observed. The comparison of the optical pulse shape of the Crab pulsar with the Jodrell Bank radio ephemerides shows that the optical pulse leads the radio one by hundreds of μs.

As previously demonstrated, in the spacecraft position determination process the accuracy depends mainly on the uncertainty of the phase of the main peak of the light curve. The uncertainty of the phase peak is due to the timing noise of the pulsar. The pulsars' periodic signals have timing stabilities comparable to atomic clocks, but there are some time irregularities. Among all the different type of irregularities the most important for our purpose is the red noise component of the pulsar timing noise which is the component that cannot be easily suppressed or modelled.

By making a complete long-term phase analysis it is possible to give a more accurate prediction of the spin evolution of pulsars by reducing the impact of the timing noise. In order to reduce the impact of the timing noise in the accuracy of the position determination, an alternative to the determination of the phases, which is complex and takes time, is to reduce the observation time. During long-term observations the red noise component of the pulsars timing noise becomes more important. The idea is that by observing the Crab pulsar with short observation times, it is possible to reduce the impact of the timing noise. This can lead to greater accuracy of the navigation solution.

The data of the Crab pulsar are those taken with the 1.82 m Copernicus telescope in Asiago, which is much larger than a feasible satellite telescope. A further analysis to determine the ideal dimensions of an optical pulsars navigation system telescope would be required, but this was not the purpose of the thesis.
The Crab pulsar has been observed starting at 20:24 on January 19, 2018 with the very fast optical photon counter Aqueye+ [Naletto et al., 2013], [Zampieri et al., 2015], an instrument already described (see Chapter 5). Aqueye+ is equipped with SPAD detectors and permits to record and store arrival times of all detected photons with an absolute precision better than 500 ps for hour-long observing sessions. The data used in the analysis cover 90 mins of observation time. The time tags of the detected photons have been reduced to the SSB using Tempo2 software. The software, already described in Chapter 5, needs the observatory position as input parameter. We have exploited this fact in the following analysis, assuming the observatory in Asiago as our satellite rotating around the Sun following the orbit of the Earth. The baricentrization of the time of arrival of each detected photon is the fundamental step to reconstruct the correct pulse profile of the pulsar. The correct baricentrization is performed if the input three dimension position of the observatory is correct. If the input position is not correct the pulse shape of the pulsar shows differences from the one obtained with the correct baricentrization. As already explained in Chapter 4, the way the pulse profile differences are going to be measured gives rise to the different positioning methods. The ToA method measures the phase shift, $\Delta\phi$, of the main peak due to the light travel time delay between estimated and true position, while the SEPO method measures the decrease of the significance, χ^2 value, due to the decrease of the sharpness of the pulse shape with respect to the correct one. To carry out these measurements for the two methods we baricentered each time-tagged photon first with the correct and then with a wrong position of the observatory as input parameters of Tempo2 software.
The aim of this analysis is to check the feasibility of the two different methods (ToA and SEPO) and to estimate what could potentially be the positioning accuracy. Considering that the Crab pulsar is the best candidate of an optical pulsar navigation system we used the available data to reach the purpose. In order to measure the differences between the measured pulse shape and the template of the pulse shape we needed to find the method to obtain the two pulse shapes, one correct and one distorted. The idea was to use the baricentrization to create a different pulse shape. In order to obtain the pulse shape from the baricentrized photons of the Crab pulsar it is necessary to perform the binning and the epoch-folding of the

data, as already described in Chapter 2. *Xronos*[1] is the timing analysis software package used to carry out the analysis here reported. In detail, the used Xronos tools are $efsearch$ and $efold$. $efsearch$ permits to find the period of a periodic time series; it needs as input the time series of the observation, an initial period trial value, the number of phase bin per period and the required resolution of the period search. As output it gives the value of the period at the required resolution and the plot of the χ^2 versus the period. The search of the period can be pursued several times changing the initial value of the period and the searched resolution of the period determination. Ideally, the period can be searched with accuracy of ns or even better. The problem is that at a certain point the χ^2 plot starts to oscillate and the determination of the centroid is no longer accurate, so defining the limiting time resolution of the period determination. After the determination of the period using $efsearch$, it is possible to determine the light curve of the pulsar using the Xronos tool $efold$. $efold$ permits to find the pulse profile of a periodic time series and it needs as input the time series of the observation, the correct folding period which is taken from the result of the $efsearch$ task, and the chosen phase bin per period. By folding the time series within the correct period, $efold$ gives in output the pulse profile of the pulsar and the relative error in counts per second. It is possible, if necessary, to consider the first time derivative of the period of the pulsar in both the routines ($efsearch$ and $efold$) in order to consider the phase evolution of the pulsar.

After determining the correct and the distorted pulse shape of the pulsar it is possible to carry out the analysis using the two different position determination methods.

7.2 Phase measurements

In this section the results of the ToA method are reported. By using one pulsar it is possible to determine the delta correction along the line of sight of the pulsar. The timing residual obtained by comparing the correct pulse profile and the distorted pulse profile is equivalent to determining the light travel time delay between the estimated and true position along the line of sight of the pulsar. The purpose of this analysis was to verify if it is possible to reach accuracy better than 10 km by using a short observation time.

The first step of this analysis is the determination of the position of the main peak in the different cases to make the comparison possible. In order to define the phase of the main peak it is necessary to fit the pulse profile. The analytic template calculated with the sum of sixteen Lorentzians that fits the pulse shape of the Crab pulsar is taken from Zampieri et al. [2014] and it is given by the following equation

$$f(x) = p \sum_{i=1}^{16} \frac{d_{i-1} b_i^2}{b_i^2 + (x - x_1 + h_{i-1})^2} + q \tag{7.1}$$

where p, q, x_1 are free parameters and b_i, d_{i-1} and h_{i-1} are reported in Table 7.1 with i ranging from 1 to 16. The fitting parameters are the total amplitude p, the

[1] https://heasarc.gsfc.nasa.gov/docs/xanadu/xronos/xronos.html

background level q and the phase of the main peak x_1. Figure 7.1 shows the analytic template obtained with equation (7.1). The fit of the analytic template with the data

Parameter	Value	Parameter	Value	Parameter	Value
b_1	0.0146996	d_0	1	h_0	0
b_2	0.0146996	d_1	0.217538	h_1	0.0295389
b_3	0.0146996	d_2	0.120438	h_2	0.0452724
b_4	0.0146996	d_3	0.343795	h_3	0.0159706
b_5	0.0146996	d_4	0.0274555	h_4	-0.0405742
b_6	0.00390605	d_5	0.104503	h_5	-0.004064
b_7	0.0131649	d_6	0.0524991	h_6	-0.408426
b_8	0.0517911	d_7	0.0462601	h_7	-0.493455
b_9	0.0386609	d_8	0.250336	h_8	-0.400741
b_{10}	0.0377745	d_9	0.063293	h_9	-0.445372
b_{11}	0.0156592	d_{10}	-0.0323015	h_{10}	0.0948912
b_{12}	0.0325165	d_{11}	-0.0176647	h_{11}	0.133417
b_{13}	0.0531056	d_{12}	0.0128576	h_{12}	0.355586
b_{14}	0.209385	d_{13}	0.00944315	h_{13}	-0.0200141
b_{15}	-0.0630249	d_{14}	-0.00883256	h_{14}	-0.261205
b_{16}	0.0259154	d_{15}	-0.00388652	h_{15}	-0.153419

Table 7.1: Values for the analytic template adopted to fit the Crab pulse shape from Zampieri et al. [2014].

has been carried out using a non-linear fitting tool *Scipy.optimize.curve_fit*[2] which is a package of the computational environment *python*[3]. This is a Scipy package which uses the non-linear least squares to fit a function to data. In order to perform the analysis, the data have been baricentrized considering the correct position of the observatory and considering the position shifted in the three dimensions of 100, 1000 and 3000 metres with respect to the corrected one. They are all reported in Table 7.2. After baricentrization, the Crab period has been estimated using Xronos's task

Geocentric Coordinates		
x [m]	y[m]	z[m]
4360966.0	892728.1	4554543.1

Table 7.2: Correct geocentric coordinates of the 182 cm Copernicus telescope in Asiago; the uncertainty is 0.3 m (3σ) [Germanà et al., 2012].

$efsearch$ with a resolution of 100 ps: $P_{ini} = 0.0337445820s$. Then, using Xronos's task $efold$, the light curve of the Crab pulsar has been calculated considering the data baricentered with different positions. In 30 mins of observation time the intrinsic slow down behaviour of the pulsar is enough to hinder the measurement of the shift among the different positions of the observatory. In fact, the intrinsic phase shift due to the slow down of the Crab after 30 mins is ~ 0.001 ($\Delta\phi = 0.5\dot{\nu}\Delta t^2$) considering the first period derivative of the Crab $dP/dt = 4.2074026e-13$ s/s, measured in the

[2]https://docs.scipy.org/doc/scipy/reference/generated/scipy.optimize.curve_fit.html
[3]https://www.python.org/

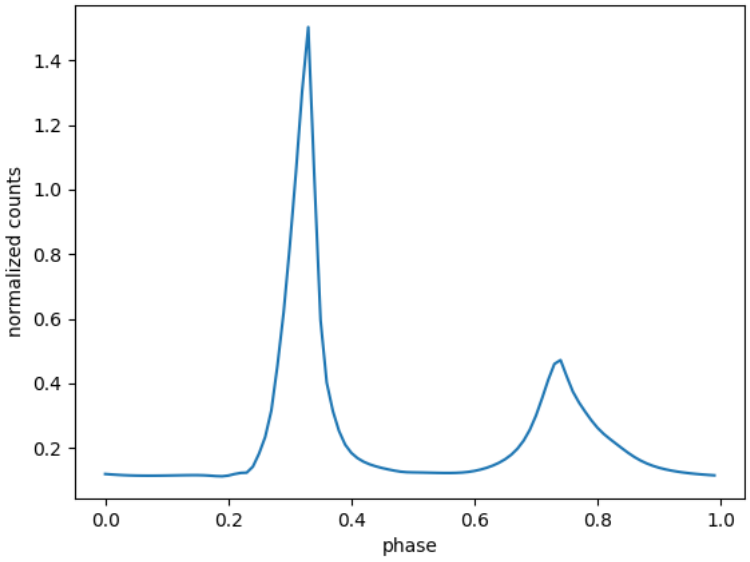

Figure 7.1: Analytic template of the Crab pulse shape obtained with function (7.1).

radio band at the time of the optical observations and reported in the Jodrell Bank monthly ephemeris. The intrinsic shift is not negligible compared to the expected shift due to the position. As a result we had to consider also the first period derivative to achieve the necessary accuracy to perform the analysis. The period derivative can be determined by making a phase analysis which means calculating a phase coherent timing solution in different observing runs in order to determine the evolution of the phase. Here we adopted a simplified approximate approach using the value of $\dot{P}$ reported in the Jodrell Bank radio ephemeris. Although it is derived from an average of radio measurements taken on longer time intervals, variations of the first time derivative over a few days are usually not very pronounced (on the second decimal digit). This level of accuracy is sufficient for our purposes. The results of the fit are reported in Tables 7.3, for 1000 phase bins, and 7.4, for 10000 phase bins. In the two tables the first three values are the ones corresponding to 30 mins of observation time while the last three values are the ones corresponding to 90 mins of observation time. All three parameters of the fit are reported for completeness, but actually we are interested only in the value of x_1, the phase of the main peak.

The reported uncertainties are estimated from the square-root of the diagonal values of the covariance matrices resulting from the fit. The errors for the pulse shape with 10000 phase bins per period are smaller than the error for the pulse profile with 1000 phase bins per period. The reason is that the pulse profile with 10000 phase bins has better resolution in phase, while maintaining a good counting statistics per bin.

In order to check that Xronos correctly takes into account the derivative of the period, we made the comparison between the non-shifted baricentrized data obtained with the 90 mins and the 30 mins of observation time. As it can be seen from Table 7.5 the value of the phase difference $\Delta\phi$ is consistent within 4σ in both

Results of the fit for 1000 phase bins			
30 mins	p	q	x_1
non shifted	1.2670 ± 0.0018	0.84420± 0.00033	0.317037± 0.000037
shifted 100m	1.2670± 0.0018	0.84420± 0.00033	0.317047± 0.000037
shifted 1000m	1.2670± 0.0018	0.84420± 0.00032	0.317130± 0.000036
shifted 3000m	1.2670± 0.0018	0.84420± 0.00032	0.317317± 0.000036
90 mins	p	q	x_1
non shifted	1.3038± 0.0013	0.83972± 0.00024	0.317200± 0.000026
shifted 100m	1.3038± 0.0013	0.83972±0.00024	0.317210± 0.000026
shifted 1000m	1.3038± 0.0013	0.83972± 0.00024	0.317289± 0.000026
shifted 3000m	1.3039± 0.0013	0.83971± 0.00024	0.317467± 0.000026

Table 7.3: Results of the fit of the pulse profile with 1000 phase bins. The non-shifted values are intended the results of the fit considering the correct obtained using the function reported in equation 7.1, while the other refer to a shift of 100, 1000 and 3000 m with respect to the correct position.

Results of the fit for 10000 phase bins			
30 mins	p	q	x_1
non shifted	1.2670 ±0.0016	0.84363±0.00029	0.317037±0.000032
shifted 100m	1.2670±0.0016	0.84363±0.00029	0.317046±0.000032
shifted 1000m	1.2670±0.0016	0.84362±0.00029	0.317129±0.000032
shifted 3000m	1.2670±0.0016	0.84363±0.00029	0.317316±0.000036
90 mins	p	q	x_1
non shifted	1.30386 ± 0.00094	0.83952± 0.00017	0.317199± 0.000019
shifted 100m	1.30387± 0.00094	0.83953± 0.00017	0.317208± 0.000019
shifted 1000m	1.30287± 0.00094	0.83953± 0.00017	0.317288± 0.000019
shifted 3000m	1.30386± 0.00094	0.83953± 0.00017	0.317467± 0.000019

Table 7.4: Results of the fit of the pulse profile with 10000 phase bins. The non-shifted values are intended the results of the fit considering the correct obtained using the function reported in equation 7.1, while the other refer to a shift of 100, 1000 and 3000 m with respect to the correct position.

cases (1000 and 10000 phase bins per period). We do not consider the lack of the agreement at the 3σ level particularly significant because we did not consider the correlation of the paramenters p, q and x_1 in the covariance matrix. In any case, only performing a full phase analysis we will be able to determine the phase of the main peak with greater precision, by determining in a self-consistent way the period derivative from the optical data. After this check we then measured the phase

Comparison between the non-shifted phase measurements					
90 mins	$\Delta\phi$	1σ	2σ	3σ	4σ
1000 phase bins	0.00016262	0.000045	0.000091	0.00014	0.00018
30 mins	$\Delta\phi$	1σ	2σ	3σ	4σ
10000 phase bins	0.00016227	0.000038	0.000075	0.00011	0.00015

Table 7.5: Comparison of the values of x_1 obtained from the fits of the non-shifted baricentered data. Here, $\Delta\phi$ is intended as the difference of the phase measured in 90 mins and 30 mins of observation time.

shift due to the incorrect input position of the observatory in the baricenterization. The analysis reported in Chapter 6 showed that the achievable accuracy of the ToA method is of 10 km at most considering the epoch-by-epoch approach. In this analysis we have the possibility to verify this a-priori analysis result considering real data. Tables 7.6 and 7.7 report the results of the phase measurement method. The results

Phase shift measurement (30 *mins* **of observation time)**					
1000 bins	$\Delta\phi$	1σ	2σ	3σ	4σ
$100m$	0.0000094	0.000052	0.00010	0.00016	0.00021
$1000m$	0.000093	0.000052	0.00010	0.00016	0.00021
$3000m$	0.00028	0.000052	0.00010	0.00016	0.00021
10000 bins	$\Delta\phi$	1σ	2σ	3σ	4σ
$100m$	0.0000092	0.000046	0.000091	0.00014	0.00018
$1000m$	0.000089	0.000046	0.000092	0.00014	0.00018
$3000m$	0.00028	0.000046	0.000092	0.00014	0.00018

Table 7.6: Phase difference $\Delta\phi$ between the shifted value and the non shifted one, considering 30 mins of observation time.

Phase shift measurement (90 *mins* **of observation time)**					
1000 bins	$\Delta\phi$	1σ	2σ	3σ	4σ
$100m$	0.0000091	0.000037	0.000075	0.00011	0.00015
$1000m$	0.000089	0.000037	0.000074	0.00011	0.00015
$3000m$	0.00027	0.000037	0.000074	0.00011	0.00015
10000 bins	$\Delta\phi$	1σ	2σ	3σ	4σ
$100m$	0.0000089	0.000027	0.000054	0.000080	0.00011
$1000m$	0.000089	0.000027	0.000054	0.000080	0.00011
$3000m$	0.00027	0.000027	0.000054	0.000080	0.00011

Table 7.7: Phase difference $\Delta\phi$ between the shifted value and the non shifted one, considering 90 mins of observation time.

obtained considering 90 and 30 mins of observation time and 1000 and 10000 phase bins are consistent with each other within the errors. In the case of the shift from the correct position of 3000 m the phase shift is measurable with a small relative error. For the 100 m and 1000 m displacements the phase shift is not significant (smaller than the error). The error has been calculated summing in quadrature the two error measurements. We can conclude that the real data analysis for the phase measurement method gives results in line with the accuracy analysis performed in Chapter 6, and that it is possible to measure the position of the spacecraft with an accuracy of 3000 m. The two points to be improved in the present analysis are the following. We considered observations obtained with a telescope with a diameter of 182 cm, which is much larger than a telescope that a spacecraft can have on board. The other point is the assumption concerning the period derivative. The proper way to carry out this analysis would require the phase analysis to determine the period derivative self-consistently. In this way the results reported in Table 7.5 would probably be consistent within 3σ.

7.3 Significance Analysis

SEPO (Significance Enhancement of Pulse profile with Orbit-dynamics) method, described in Section 4, permits to determine the orbital parameters of the spacecraft using only one pulsar. The basic concept of this method is that the observed pulse profile will be slightly distorted for inaccurate input orbital parameters. The deformation of the pulse profile is directly connected with a certain decrease of the significance of the profile signal. We carried out this analysis in a way similar to what we have been done previously for the phase measurement method. The baricenterization has been performed considering as input in Tempo2 the correct coordinates of the observatory and various different incorrect coordinates. The incorrect coordinates are determined considering positive and negative shifts from the correct position.
The aim of this analysis was to verify that with only 90 mins of observation of the Crab pulsar it is possible to observe a detectable decrease of the χ^2 value in the various cases with respect to the case of the correct baricenterization.

There are several steps to perform in this analysis. The first is the determination of the baricentered data considering the correct and incorrect position as input parameters in the Tempo2 software. The considered data are those obtained in 90 mins of observation, because the statistics of the data obtained within 30 mins of observation was too low. The shifts considered in this analysis are: +100, −100, +300, −300, +1000, −1000, +3000 and −3000 metres, with equal increments along the three spatial directions. The second step is the determination of the χ^2 for the time series. The χ^2 plot is an output of the $efold$ Xronos's task. The value we are interested in is the maximum centroid value of the χ^2 curve for each dataset. The folding has been performed considering 10000 phase bins per period. The maximum values of the χ^2 for the different shifts are reported in Table 7.8. The maximum

Variation of the χ^2	
Shift [m]	χ^2
-3000	4.10928100E+06
-1000	4.10930075E+06
-300	4.10951200E+06
-100	4.10955675E+06
0	4.10961825E+06
+100	4.10961400E+06
+300	4.10958575E+06
+1000	4.10965700E+06
+3000	4.10958575E+06

Table 7.8: Maximum χ^2 values for the different shifts.

value of the χ^2 tends to decrease gradually for larger shifts as expected. In order to determine the accuracy of the method, a Gaussian fit to the data has been performed. The fit of the Gaussian function with the data has been carried out using a non-linear fit tool *Scipy.optimize.curve_fit* which is a package of the computational

environment *python*. This package is a Scipy package which uses the non-linear least squares to fit a function to data. The data values and the Gaussian fit are plotted in Figure 7.2. The results show that there is an significant statistical noise that makes

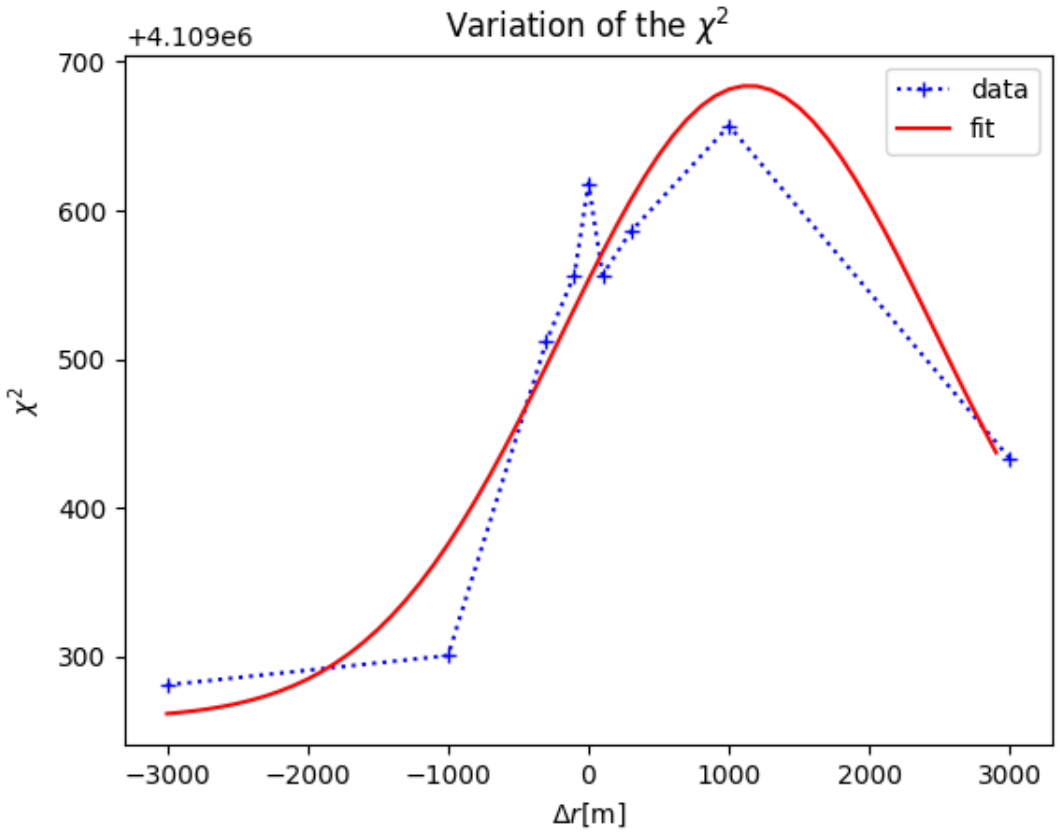

Figure 7.2: Variation of the χ^2 versus the shift, Δr, from the input position adopted for the baricenterization of the data of the Crab pulsar. The value are obtained considering 90 mins of observation time with the Aqueye+ mounted at the Copernicus telescope of the Asiago observatory.

the obtained curve deviate from the expectations. For example, the χ^2 value for the +1000 m shift is larger than the unshifted one. This statistical noise can be reduced by considering a longer observation time. By considering a longer observation time the number of detected photons would be greater but probably the red noise of the pulsar would become more important and consequently the solution to the problem would be a complete analysis of the evolution of the phases.
The uncertainty of the method is conservatively approximated taking the dispersion of the Gaussian distribution. In this analysis the dispersion of the distribution is equal to 1335 m. The most important result of this analysis is the fact that with only 90 mins of observation time it is possible to measure the decrease of the χ^2 value due to the distorted profile. The only previous analysis of this type is the one reported by Zheng et al. [2019]. It is not possible to directly compare the two results because they used the orbital parameters to derive the position of the spacecraft and the accuracy of the method while in our case we measured a deviation from the correct position considering the Cartesian coordinates of an observatory on Earth. However, by observing the X-ray emission of the Crab pulsar for a five-day period

the accuracy they obtained for position and velocity of the spacecraft is 10 km (3σ) and 10 m/s(3σ) respectively. In the case of the optical emission the statistics is much larger compared to the X-ray emission. For this reason it is possible to obtain enough counts with a shorter observation time and it is possible to measure the decrease of the χ^2 value due to the distorted profile even with only 90 mins of observation time.

8. Conclusions

The aim of the thesis was assessing the feasibility of a satellite navigation system which makes use of optical pulsars as natural navigation beacons. The main result is that optical pulsar navigation is possible using two different methods: phase measurement and significance analysis. The achievable accuracy has been determined using two estimation theories. The two analyses show that the achievable accuracy for the phase measurements methods is limited by the uncertainty of the peak phase determination, which is $\sim 30\mu$s. The WLS analysis allows to achieve an accuracy of 10 km for the position determination. By considering an iterative approach, using the Kalman filter, we obtained $\sim 5 \times 10^2$ m after 20 days of observation with a sampling time of 10 s. The real data analyses use the Crab data obtained with Aqueye+ mounted at the 182 cm Copernicus telescope in Asiago. In this case both navigation methods were considered. The results for the phase measurement method show that it is possible to observe a shift of 3000 m with respect to the correct position. The SEPO method suggests an accuracy of $\sim$1335 m in only 90 mins of observation time. The limiting factor of this method is the statistics. A high statistic is needed to get good results. The most important problem of navigation systems which use pulsar as navigation beacons is the intrinsic timing noise of the pulsars. This intrinsic timing noise can be reduced by observing the pulsar for less time or by performing a complete phase analysis. The high statistics characteristic of the optical band is the key to understand the proposal for satellite navigation using optical emission of pulsars. This thesis work is only a first study on navigation with optical pulsars. Actually, it would be necessary to perform a further study regarding the ideal dimension and optical design of the navigation instrument. Furthermore, to determine if it is possible to obtain a better accuracy than that resulting from the analyses performed in this study it will be necessary to do a complete study of the evolution of the pulsars phases.

Bibliography

F. Ambrosino, A. Papitto, L. Stella, F. Meddi, P. Cretaro, L. Burderi, T. Di Salvo, G. L. Israel, A. Ghedina, L. Di Fabrizio, and L. Riverol. Optical pulsations from a transitional millisecond pulsar. *Nature Astronomy*, 1:854–858, Oct 2017. doi: 10.1038/s41550-017-0266-2.

W. Baade and F. Zwicky. Remarks on super-novae and cosmic rays. *Phys. Rev.*, 46: 76–77, Jul 1934. doi: 10.1103/PhysRev.46.76.2. URL `https://link.aps.org/doi/10.1103/PhysRev.46.76.2`.

C. Barbieri, G. Naletto, T. Occhipinti, C. Facchinetti, E. Verroi, E. Giro, A. Paola, S. Billotta, P. Zoccarato, P. Bolli, F. Tamburini, G. Bonanno, M. D'Onofrio, S. Marchi, G. Anzolin, I. Capraro, F. Messina, M. Belluso, C. Pernechele, and F. Pedichini. Aqueye, a single photon counting photometer for astronomy. *Journal of Modern Optics*, 56:261–272, 01 2009. doi: 10.1080/09500340802450565.

F.H. Bauer, K. Hartman, and E.G. Lightsey. Spaceborne gps current status and future visions. *in Aerospace Conference*, 3 (IEEE):195–208, 1998 IEEE.

W. Becker, M. G. Bernhardt, and A. Jessner. Autonomous Spacecraft Navigation With Pulsars. *Acta Futura*, 7:11–28, Nov 2013.

P.A. Caraveo, G.F. Bignami, and S. Mereghetti. A Candidate Identification for PSR 0656+14 and the Optical Emission from Isolated Neutron Stars. 422:L87, Feb 1994. doi: 10.1086/187219.

T. J. Chester and S. A. Butman. Navigation using X-ray pulsars. In *The Telecommunication and Data Acquisition Report*, pages 22–25, Jun 1981.

W. J. Cocke, M. J. Disney, and D. J. Taylor. Discovery of Optical Signals from Pulsar NP 0532. *nature*, 221(5180):525–527, Feb 1969. doi: 10.1038/221525a0.

X. P. Deng, G. Hobbs, X. P. You, M. T. Li, M. J. Keith, R. M. Shannon, W. Coles, R. N. Manchester, J. H. Zheng, X. Z. Yu, D. Gao, X. Wu, and D. Chen. Interplanetary spacecraft navigation using pulsars. *Advances in Space Research*, 52(9): 1602–1621, Nov 2013. doi: 10.1016/j.asr.2013.07.025.

G.S. Downs. Interplanetary Navigation Using Pulsating Radio Sources. *National Aeronautics and Space Administration*, 1974.

A.A. Emadzadeh and J. Speyer. *Navigation in Space by X-ray Pulsars.* Springer, 2010.

Fermi LAT Collaboration, M. Ackermann, A. Albert, L. Baldini, J. Ballet, G. Barbiellini, C. Barbieri, D. Bastieri, R. Bellazzini, E. Bissaldi, R. Bonino, E. Bottacini, T. J. Brand t, J. Bregeon, P. Bruel, R. Buehler, G. A. Caliand ro, R. A. Cameron, P. A. Caraveo, C. Cecchi, E. Charles, A. Chekhtman, C. C. Cheung, J. Chiang, G. Chiaro, S. Ciprini, J. Cohen-Tanugi, A. Cuoco, S. Cutini, F. D'Ammando, F. de Palma R. Desiante, S. W. Digel, L. Di Venere, P. S. Drell, C. Favuzzi, S. J. Fegan, E. C. Ferrara, A. Franckowiak, S. Funk, P. Fusco, F. Gargano, D. Gasparrini, N. Giglietto, F. Giordano, G. Godfrey, I. A. Grenier, M. H. Grondin, J. E. Grove, L. Guillemot, S. Guiriec, K. Hagiwara, A. K. Harding, E. Hays, J. W. Hewitt, A. B. Hill, D. Horan, T. J. Johnson, J. Knödlseder, M. Kuss, S. Larsson, L. Latronico, M. Lemoine-Goumard, J. Li, L. Li, F. Longo, F. Loparco, M. N. Lovellette, P. Lubrano, S. Maldera, A. Manfreda, F. Marshall, P. Martin, M. Mayer, M. N. Mazziotta, P. F. Michelson, N. Mirabal, T. Mizuno, M. E. Monzani, A. Morselli, I. V. Moskalenko, S. Murgia, G. Naletto, E. Nuss, T. Ohsugi, M. Orienti, E. Orlando, D. Paneque, M. Pesce-Rollins, F. Piron, G. Pivato, T. A. Porter, S. Rainò, R. Rando, M. Razzano, A. Reimer, O. Reimer, T. Reposeur, R. W. Romani, P. M. Saz Parkinson, A. Schulz, C. Sgrò, E. J. Siskind, D. A. Smith, F. Spada, G. Spandre, P. Spinelli, D. J. Suson, H. Takahashi, J. B. Thayer, D. J. Thompson, L. Tibaldo, D. F. Torres, Y. Uchiyama, G. Vianello, K. S. Wood, M. Wood, and L. Zampieri. An extremely bright gamma-ray pulsar in the Large Magellanic Cloud. *Science*, 350(6262):801–805, Nov 2015. doi: 10.1126/science.aac7400.

C. Germanà, L. Zampieri, C. Barbieri, G. Naletto, A. Čadež, M. Calvani, M. Barbieri, I. Capraro, A. Di Paola, C. Facchinetti, T. Occhipinti, A. Possenti, D. Ponikvar, E. Verroi, and P. Zoccarato. Aqueye optical observations of the Crab Nebula pulsar. 548:A47, Dec 2012. doi: 10.1051/0004-6361/201118754.

P. Ghosh and F. K. Lamb. Diagnostics of disk-magnetosphere interaction in neutron star binaries. *NASA STI/Recon Technical Report A*, 93:487–510, Jan 1992.

P. Giordano, P. Zoccarato, M. Otten, and M. Crisci. P2OD: Real-time Precise Onboard Orbit Determination for LEO Satellites. *Proceedings of the 30th International Technical Meeting of the Satellite Division of The Institute of Navigation (ION GNSS+ 2017)*, pages 1754–1771, Sep 2017. doi: /10.33012/2017.15190.

T. Gold. Rotating Neutron Stars as the Origin of the Pulsating Radio Sources. *Nature*, 218(5143):731–732, May 1968. doi: 10.1038/218731a0.

S. Gradari, M. Barbieri, C. Barbieri, G. Naletto, E. Verroi, T. Occhipinti, P. Zoccarato, C. Germana, and A. Possenti. The optical light curve of the lmc pulsar b0540-69 in 2009. 12 2010.

P.H. Graven, J.T. Collins, S.I. Sheikh, and J.E. Hanson. Spacecraft navigation using x-ray pulsars. 7, Tralee, County Kerry Ireland, 6 2008. GNC.

A. Hewish, S.J. Bell, J.D.H. Pilkington, P.F. Scott, and R.A. Collins. Observation of a Rapidly Pulsating Radio Source. *Nature*, 1968.

G. Hobbs, R. Edwards, and R. Manchester. TEMPO2: a New Pulsar Timing Package. *Chinese Journal of Astronomy and Astrophysics Supplement*, 6(S2):189–192, Dec 2006.

G. Hobbs, A. G. Lyne, and M. Kramer. An analysis of the timing irregularities for 366 pulsars. 402(2):1027–1048, Feb 2010. doi: 10.1111/j.1365-2966.2009.15938.x.

R. Kaune. Accuracy Studies for TDOA and TOA Localization. 2012.

B. Kern, C. Martin, B. Mazin, and J. P. Halpern. Optical Pulse-Phased Photopolarimetry of PSR B0656+14. 597(2):1049–1058, Nov 2003. doi: 10.1086/378670.

A. Lawrence. An Outline of Inertial Navigation. *in Modern Inertial Technology, Springer*, pages 4–24, 1998.

W. R. Leeb, J. Alves, S. Meingast, and M. Brunner. Simulated low-intensity optical pulsar observation with single-photon detector. *aap*, 574:A9, Feb 2015. doi: 10.1051/0004-6361/201424480.

A. G. Lyne, R. S. Pritchard, and F. Graham Smith. 23 years of Crab pulsar rotational history. 265:1003–1012, Dec 1993. doi: 10.1093/mnras/265.4.1003.

M. Marisaldi, P. Maccagnani, F. Moscatelli, C. Labanti, F. Fuschino, M. Prest, A. Berra, D. Bolognini, M. Ghioni, I. Rech, A. Gulinatti, and A. Giudice. Single photon avalanche diodes for space applications. *IEEE Nuclear Science Symposium Conference Record*, 10 2011. doi: 10.1109/NSSMIC.2011.6154465.

R. Mignani, P. Caraveo, and G. Bignami. Geminga, 10 years of optical observations. *The Messenger*, 76:32–34, 05 1994.

R. P. Mignani, P. A. Caraveo, and G. F. Bignami. Optical observations of pulsars: the ESO contribution. *The Messenger*, 99:22–26, Mar 2000.

J.W. Mitchell, M.A. Hassouneh, L.M.B. Winternitz, J.E. Valdez, S.R. Price, W.H. Semper S.R., Yu, Z. Arzoumanian, P.S. Ray, K.S. Wood, R.J. Litchford, and K.C. Gendreau. Sextant-station explorer for x-ray timing and navigation technology. *American Institute of Aeronautics and Astronautics*, 2015.

G. Naletto, C. Barbieri, T. Occhipinti, I. Capraro, A. di Paola, C. Facchinetti, E. Verroi, P. Zoccarato, G. Anzolin, M. Belluso, S. Billotta, P. Bolli, G. Bonanno, V. da Deppo, S. Fornasier, C. Germanà, E. Giro, S. Marchi, F. Messina, C. Pernechele, F. Tamburini, M. Zaccariotto, and L. Zampieri. Iqueye, a single photon-counting photometer applied to the ESO new technology telescope. *aap*, 508(1):531–539, Dec 2009. doi: 10.1051/0004-6361/200912862.

G. Naletto, C. Barbieri, E. Verroi, M. Zaccariotto, F. Romanato, A. Sponselli, E. Mari, M. Barbieri, L. Zampieri, T. Occhipinti, I. Capraro, and A. Cardullo. Aqueye plus: A very fast single photon counter for astronomical photometry to quantum limits equipped with an optical vortex coronagraph. *Proc SPIE*, 8875, 09 2013. doi: 10.1117/12.2022571.

A. Papitto, F. Ambrosino, L. Stella, D. Torres, F. Coti Zelati, A. Ghedina, F. Meddi, A. Sanna, P. Casella, Y. Dallilar, S. Eikenberry, G. L. Israel, F. Onori, S. Piranomonte, E. Bozzo, L. Burderi, S. Campana, D. de Martino, T. Di Salvo, C. Ferrigno, N. Rea, A. Riggio, S. Serrano, A. Veledina, and L. Zampieri. Pulsating in Unison at Optical and X-Ray Energies: Simultaneous High Time Resolution Observations of the Transitional Millisecond Pulsar PSR J1023+0038. *apj*, 882 (2):104, Sep 2019. doi: 10.3847/1538-4357/ab2fdf.

J.A. Sala, X. Urruela, R. Villares, Estalella, and J.M. Paredes. Feasibility Study for a Spacecraft Navigation System Relying on Pulsar Timing Information. *European Space Agency, the Advanced Concepts Team*, 03-4202, 2004.

J.A. Sala, X. Urruela, Andreu, Villares, Xavier, J. Romeu, R. Estalella, and J. Paredes. Pulsar Navigation. 03 2008.

S. L. Shapiro and S. A. Teukolsky. Book-Review - Black-Holes White Dwarfs and Neutron Stars. *Journal of the British Astronomical Association*, 93(6):276, Oct 1983.

S.I. Sheikh, D.J. Pines, P.S. Ray, K.S. Wood, M.N. Lovellette, and M.T. Wolff. Spacecraft Navigation Using X-Ray Pulsars. *Journal of Guidance Control Dynamics*, 29(1):49–63, Jan 2006. doi: 10.2514/1.13331.

S. Shemar, G. Fraser, L. Heil, D. Hindley, A. Martindale, P. Molyneux, J. Pye, R. Warwick, and A. Lamb. Towards practical autonomous deep-space navigation using X-Ray pulsar timing. *Experimental Astronomy*, 42(2):101–138, Oct 2016. doi: 10.1007/s10686-016-9496-z.

S. Shemar, G. Fraser, L. Heil, D. Hindley, A. Martindale, P. Molyneux, J. Pye, R. Warwick, and A. Lamb. Towards practical autonomous deep-space navigation using x-ray pulsar timing. *Experimental Astronomy*, 42, 07 2016. doi: 10.1007/s10686-016-9496-z.

A. Spolon, A. Burtovoi, G. Naletto, C. Barbieri, M. Barbieri, A. Patruno, and E. Verroi. Timing analysis and pulse profile of the vela pulsar in the optical band from iqueye observations. *Monthly Notices of the Royal Astronomical Society*, 482: 175–183, 01 2019. doi: 10.1093/mnras/sty2605.

J.S. Subirana, J.M.J. Zornoza, and M. Hernández-Pajares. *GNSS DATA PROCESSING. Volume I: Fundamentals and Algorithms*. ESA Communications, 2013.

P.J.G. Teunissen, D.G. Simons, and C.C.J.M. Tiberius. *Probability and observation theory*. Department of Earth Observation and Space Systems (DEOS), 2008.

M. Thameemunnisha and Mankali Ramachandran. Kalman filter analysis for orbit estimation using pulsars for interplanetary missions. *IFAC-PapersOnLine*, 49: 136–141, 12 2016. doi: 10.1016/j.ifacol.2016.03.042.

C.L. Thornton and J.S. Border. Radiometric tracking techniques for deep-space navigation. *Issued by the Deep-Space Communications and Navigation Systems*, 2003.

A. Čadež, L. Zampieri, C. Barbieri, M. Calvani, G. Naletto, M. Barbieri, and D. Ponikvar. What brakes the Crab pulsar? 587, Mar 2016. doi: 10.1051/0004-6361/201526490.

P. T. Wallace, B. A. Peterson, P. G. Murdin, I. J. Danziger, R. N. Manchester, A. G. Lyne, W. M. Goss, F. G. Smith, M. J. Disney, K. F. Hartley, D. H. P. Jones, and G. W. Wellgate. Detection of optical pulses from the VELA PSR. *nature*, 266: 692–694, Apr 1977. doi: 10.1038/266692a0.

L. Zampieri, C. Germanà, C. Barbieri, G. Naletto, A. Čadež, I. Capraro, A. di Paola, C. Facchinetti, T. Occhipinti, D. Ponikvar, E. Verroi, and P. Zoccarato. The Crab pulsar seen with AquEYE at Asiago Cima Ekar observatory. *Advances in Space Research*, 47(2):365–369, Jan 2011. doi: 10.1016/j.asr.2010.07.016.

L. Zampieri, A. Čadež, C. Barbieri, G. Naletto, M. Calvani, M. Barbieri, E. Verroi, P. Zoccarato, and T. Occhipinti. Optical phase coherent timing of the Crab nebula pulsar with Iqueye at the ESO New Technology Telescope. 439(3):2813–2821, Apr 2014. doi: 10.1093/mnras/stu136.

L. Zampieri, G. Naletto, C. Barbieri, E. Verroi, M. Barbieri, G. Ceribella, M. D'Alessandro, G. Farisato, A. Di Paola, and P. Zoccarato. *Aqueye+: a new ultrafast single photon counter for optical high time resolution astrophysics*, volume 9504 of *Society of Photo-Optical Instrumentation Engineers (SPIE) Conference Series*, page 95040C. 2015. doi: 10.1117/12.2179547.

L. Zampieri, A. Burtovoi, M. Fiori, G. Naletto, A. Spolon, C. Barbieri, A. Papitto, and F. Ambrosino. Precise optical timing of PSR J1023+0038, the first millisecond pulsar detected with Aqueye+ in Asiago. *mnras*, 485(1):L109–L113, May 2019a. doi: 10.1093/mnrasl/slz043.

L. Zampieri, A. Richichi, G. Naletto, C. Barbieri, A. Burtovoi, M. Fiori, A. Glindemann, G. Umbriaco, P. Ochner, V. V. Dyachenko, and M. Barbieri. Lunar Occultations with Aqueye+ and Iqueye. *aj*, 158(5):176, Nov 2019b. doi: 10.3847/1538-3881/ab3979.

S. Zheng, M. Ge, D. Han, W. Wang, Y. Chen, F. Lu, T. Bao, J. Chai, Y. Dong, M. Feng, J. He, Y. Huang, M. Kong, H. Li, L. Li, Z. Li, J. Liu, X. Liu, H. Shi, L. Song, J. Sun, R. Wang, Y. Wang, X. Wen, B. Wu, H. Xiao, S. Xiong, H. Xu, M. Xu, J. Zhang, L. Zhang, L. Zhang, X. Zhang, Y. Zhang, Y. Zhao, and S. Zhang. Test of pulsar navigation with POLAR on TG-2 space station. *Scientia Sinica Physica, Mechanica & Astronomica*, 47(9):099505, Sep 2017. doi: 10.1360/SSPMA2017-00080.

S. J. Zheng, S. N. Zhang, F. J. Lu, W. B. Wang, Y. Gao, T. P. Li, L. M. Song, M. Y. Ge, D. W. Han, Y. Chen, Y. P. Xu, X. L. Cao, C. Z. Liu, S. Zhang, J. L. Qu, Z. Chang, G. Chen, L. Chen, T. X. Chen, Y. B. Chen, Y. P. Chen, W. Cui, W. W. Cui, J. K. Deng, Y. W. Dong, Y. Y. Du, M. X. Fu, G. H. Gao, H. Gao, M. Gao, Y. D. Gu, J. Guan, C. Gungor, C. C. Guo, D. W. Han, W. Hu, Y. Huang, J. Huo, J. F. Ji, S. M. Jia, L. H. Jiang, W. C. Jiang, J. Jin, Y. J. Jin, B. Li, C. K. Li, G. Li,

M. S. Li, W. Li, X. Li, X. B. Li, X. F. Li, Y. G. Li, Z. J. Li, Z. W. Li, X. H. Liang, J. Y. Liao, G. Q. Liu, H. W. Liu, S. Z. Liu, X. J. Liu, Y. Liu, Y. N. Liu, B. Lu, X. F. Lu, T. Luo, X. Ma, B. Meng, Y. Nang, J. Y. Nie, G. Ou, N. Sai, R. C. Shang, L. Sun, Y. Tan, L. Tao, W. Tao, Y. L. Tuo, G. F. Wang, J. Wang, W. S. Wang, Y. S. Wang, X. Y. Wen, B. B. Wu, M. Wu, G. C. Xiao, S. L. Xiong, H. Xu, L. L. Yan, J. W. Yang, S. Yang, Y. J. Yang, A. M. Zhang, C. L. Zhang, C. M. Zhang, F. Zhang, H. M. Zhang, J. Zhang, Q. Zhang, T. Zhang, W. Zhang, W. C. Zhang, W. Z. Zhang, Y. Zhang, Y. Zhang, Y. F. Zhang, Y. J. Zhang, Z. Zhang, Z. Zhang, Z. L. Zhang, H. S. Zhao, J. L. Zhao, X. F. Zhao, Y. Zhu, Y. X. Zhu, and C. L. Zou. In-orbit Demonstration of X-Ray Pulsar Navigation with the Insight-HXMT Satellite. 244(1):1, Sep 2019. doi: 10.3847/1538-4365/ab3718.